Analysis of Resolved Remnants of Accreted galaxies as a Key Instrument for Halo Surveys

ESA F-MISSION

Mission classification	F-class
Proposal Acronym	ARRAKIHS
Proposal title	Analysis of Resolved Remnants of Accreted galaxies as a Key Instrument for Halo Surveys
Name and full contact information of Lead Proposer	Prof. Rafael Guzmán guzman@ifca.unican.es Instituto de Física de Cantabria (IFCA, Spain)

PHASE 2 PROPOSAL

PUBLIC VERSION

1 LIST OF CORE MEMBERS

Here we present the ARRAKIHS proposal prepared by the following mission core team, in response to the ESA F-Mission call, published on December 13, 2021:

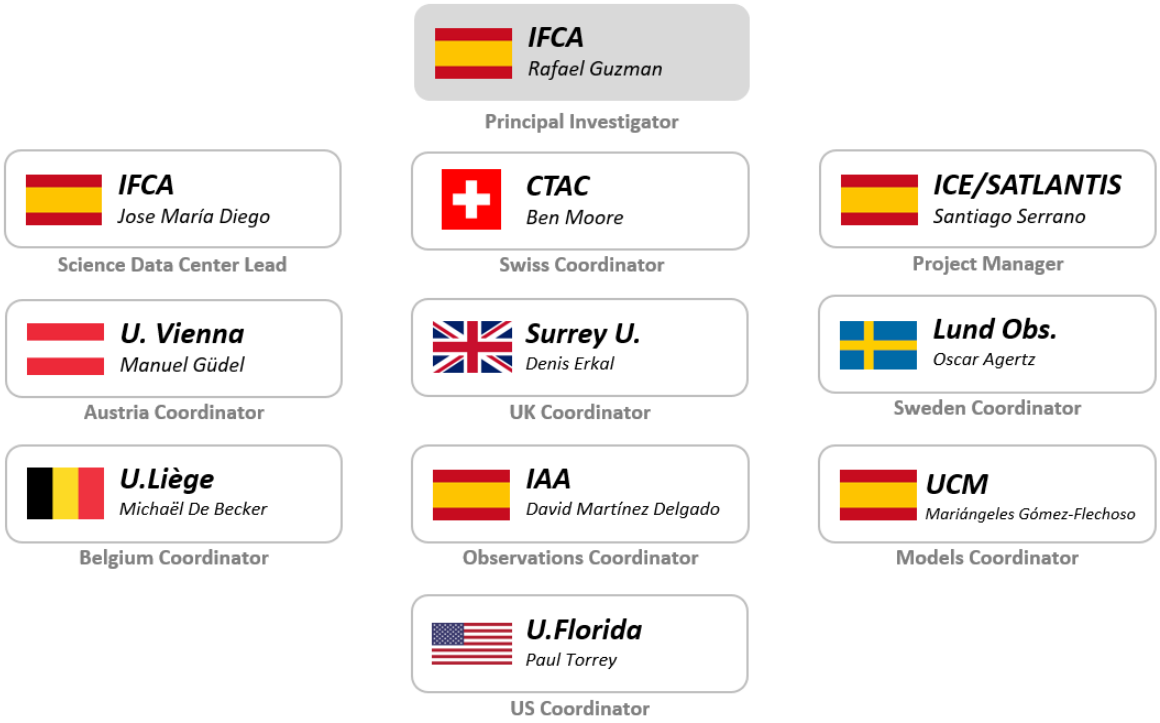

Institution Name	Researcher	E-mail address
Instituto de Física de Cantabria	Rafael Guzmán	guzman@ifca.unican.es
Universidad Complutense de Madrid	Mariángeles Gómez-Flechoso	magflechoso@ucm.es
Instituto de Astrofísica de Andalucía	David Martínez-Delgado	dmartinez@iaa.es
Center for Theoretical Astrophysics & Cosmology	Ben Moore	moore@physik.uzh.ch
Lund Observatory – Lund University	Oscar Agertz	oscar.agertz@astro.lu.se
University of Surrey	Denis Erkal	d.erkal@surrey.ac.uk
Instituto de Física de Cantabria	Jose María Diego	jdiego@ifca.unican.es
Satlantis	Santiago Serrano	serrano@satlantis.com
University of Vienna	Manuel Güdel	manuel.guedel@univie.ac.at
University of Liège	Michaël de Becker	michael.debecker@uliege.be
University of Florida	Paul Torrey	paul.torrey@ufl.edu

2 EXECUTIVE SUMMARY

The “Analysis of Resolved Remnants of Accreted galaxies as a Key Instrument for Halo Surveys” (ARRAKIHS) mission will image 50 square degrees of the sky per year down to an unprecedented ultra-low surface brightness (SB) simultaneously in two visible bands (HST F475X: 380 to 630 nm and Euclid VIS: 550 to 900 nm) and two infrared bands (Euclid Y: 920 to 1230 nm and Euclid J: 1169 to 1590 nm). These images will allow us to address major outstanding issues in the Λ-Cold Dark Matter (ΛCDM) cosmological model. In particular, if Dark Matter in our Universe deviates from the cold and collisionless model as for the standard ΛCDM, then it is expected that the satellite mass functions, satellite merger rates, and prevalence of stellar streams around dwarf galaxies would all be greatly suppressed. These observational tests could not yet be carried out because a wide field-of-view survey, imaging down to ultra-low SB limits is extremely difficult to achieve from the ground due to the atmospheric background. Instead, ARRAKIHS will use an innovative binocular telescope assembly on board a mini satellite in Low Earth Orbit. This survey will result in a first-of-its-kind catalog of ultra-low SB extragalactic images for a volume-limited and mass-limited sample of galaxies like the Milky Way in the nearby universe. The defining and unique characteristic of the ARRAKIHS mission is that it will image these systems down to an unprecedented surface brightness of 31 mag/arcsecond^2 with a resolution of 0.8 arcsec (FWHM) in visible wavelengths, and 30 mag /arcsecond^2 with 1.25 arcsec (FWHM) in the near infrared.

The ARRAKIHS mission leverages space-demonstrated technology with high Technology Readiness Level (TRL) to enter development with a very low risk posture. First, ARRAKIHS will use the binocular iSIM-170 camera which has already been validated in space and successfully demonstrated the best image quality and spatial resolution available for smallsats. The detector upgrades required for the ARRAKIHS mission are also based on flight-ready technology. The extended exposures will require a pointing stabilization upgrade that is based on the same technique already developed (to a much higher requirement) for the Euclid and CHEOPS missions. The thermo-mechanical stability of the payload and the detector cooling technology solution are also borrowed from similar solutions already developed for the Euclid and CHEOPS missions. The iSIM-170 camera can be mounted on several mini-satellite platforms which are easily adapted from successful versions currently operating in Low Earth Orbit (LEO). Finally, the state-of-the-art simulations carried out by the ARRAKIHS consortium provide a very high degree of confidence on the ability of our technology to reach the ultra-low SB levels and high spatial resolution required to successfully complete the scientific goals of the ARRAKIHS mission.

ARRAKIHS fits perfectly within ESA’s “Cosmic Vision” scientific priorities. In particular, ARRAKIHS will advance our knowledge in two of the four key questions at the heart of the “Cosmic Vision” Program: “What are the fundamental physical laws of the Universe?” and “How did the Universe originate and what is it made of?” In addition, ARRAKIHS will complement the new generation of giant ground- and space-based observatories. JWST will observe the earliest stages of galaxy formation and evolution at the highest redshift. The Rubin Observatory, Roman, and Euclid will provide images and spectra for millions of galaxies at intermediate and high redshifts. ARRAKIHS will complement these in-depth, wide-area observations of the distant universe by pioneering an unprecedented systematic exploration of the nearby universe at ultra-low SB with excellent spatial resolution from visible to infrared wavelengths.

In summary, the ESA’s F-Mission program provides a unique opportunity to carry out compelling science with a space-borne platform on a short timescale with an affordable budget. As such, we have designed the ARRAKIHS mission with three defining characteristics:

1. The ARRAKIHS mission is science focused with great potential for a major impact on our understanding of the existing tensions within modern cosmology. The core of the ARRAKIHS mission – observations of the unexplored ultra-low SB universe – can only be done from space owing to limitations on ground-based SB sensitivity due to the atmosphere. Since the science goals of this mission require to achieve a very low SB over a very wide area with ~1 arcsec resolution, there is no need for a large aperture camera. Instead, the optimum payload is a small, multispectral camera with excellent optical quality over a wide field of view.

2. The ARRAKIHS mission is designed to minimize risk. All national agencies from the participating countries in the ARRAKIHS consortium have committed to provide the necessary funds to develop the payload in collaboration between research centers and industrial partners. Major hardware for the payload will be purchased from experienced industrial partners through fixed-price contracts, thus minimizing the risk of cost overrun. Several European platform providers have confirmed their commitment to meeting the payload requirements through minor adaptations of existing platforms already validated in space. Similarly, the required orbit is very common with no major mission-specific requirements that would delay launch.

3. The ARRAKIHS mission anticipates a short timescale until launch and the beginning of space operations. Our payload and platform providers have established space heritage for the specific camera and possible platforms to be used for this mission. The heritage hardware provides credibility that the Design Reviews can be carried out on an accelerated timescale and reduces the overall schedule risk associated with satellite manufacturing and integration. The main scientific goals can be achieved within the first two years of scientific operations.

The table below summarizes the key characteristics of the ARRAKIHS mission.

MAIN SCIENCE GOALS				
• Test the predictions of the Cold Dark Matter model with unprecedented ultra-low surface brightness observations of a magnitude-limited and volume-limited sample of Milky Way-type galaxies in the local universe. • Determine the statistics and distribution of satellite galaxies down to Mv<-6 in the haloes of Milky Way-type galaxies • Determine the statistics and geometry of the stellar streams and diffuse extended light in these galaxy haloes				
SURVEY				
Sample Selection	115 MW-type galaxies from the SAGA survey between 25Mpc and 40Mpc			
	Targets	*Area*	*Dithers / Target*	*Total Integration time*
Main Sample	100 galaxy systems	160 deg2	900	150h
Duration	2 years (nominal) - 3 years (goal)			
PAYLOAD				
Telescope	Design	4x modified Maksutov-Cassegrain		
	Aperture	150 mm		
	Field-of-View	1.4 deg diameter		
Instrument Type	Visible and Infrared Imager			
Weight	50-60 kg			
Filters	HST-F475X	Euclid VIS	Euclid Y	Euclid J
Wavelengths	380 - 630 nm	550 – 900 nm	920 -1230 nm	1169 - 1590 nm
Pixel scale	1.37 arcsec		2.3 arcsec	
Coadd resolution	0.8 arcsec		1.25 arcsec	
Detector	2x Teledyne e2v 4k x 4k CCD		2x Teledyne 2k x 2k H2RG	
Operating temp	150 K		140 K	
Sensitivity	~ 31 mag/arcsec^2		~ 30 mag/arcsec^2	
SPACECRAFT				
Launcher	Vega C dedicated or Rideshare			
Orbit	Sun Synchronous Orbit LTAN 6AM/6PM from 600 to 1000 km			
Pointing	0.5 arcsec RMS over 10 minutes			
Cooling	Passive radiators and heat pipes			
Communications	Bands	S and X		
	Downlink Rate	15 Mbps		
	Daily data volume	11,1 GB		
AOCS & Propulsion	Micro Propulsion Subsystem, Reaction Wheels, Gyro Payload Fine Guidance System			
Total Wet Mass	< 300 kg			
SCHEDULE				
Mission Kick Off	*Mission Adoption*	*Launch*	*End of Observations*	
2023 Q1	2025 Q2	2029 Q3	2032 Q1	

3 SCIENCE CASE

3.1 Introduction

The Λ-Cold Dark Matter (ΛCDM) model has been used to build a remarkably clear picture of structure formation in the Universe through the collapse of primordial density fluctuations (e.g. Springel et al., 2005). This model implies the existence of a massive (i.e., *cold*) dark matter (DM) particle (e.g. Blumenthal et al., 1982) with small self-interaction cross-section (i.e., *collisionless*). In the present "precision cosmology" era, the parameters describing our universe, its composition, and its expansion can be measured in multiple ways with ever decreasing error bars.

And yet, this same ΛCDM theory – however powerful at large scales – has been demonstrated incapable of replicating some galactic-scale structures. Among the most significant discrepancies between ΛCDM models and observations are the *core-cusp* (Moore, 1994), *too- big-to-fail* (Boylan-Kolchin et al., 2011), *diversity* (e.g. Oman et al., 2015), and *missing satellites* (Klypin et al., 1999) problems (see e.g. Bullock & Boylan-Kolchin, 2017; Tulin & Yu, 2018). Each of these discrepancies reflects underlying differences in the structure, abundance, or dynamics of galaxies as modelled in ΛCDM when compared against observations. While some of these discrepancies may be addressed with strong/bursty stellar feedback, the distribution of satellite galaxies themselves has been argued to be one of the strongest tests of ΛCDM. Over half of the satellites around M31 are found to be configured into a narrow plane with line-of-sight velocities hinting that they are arranged as would be the case for a rotating structure (Kroupa et al., 2005). Such satellite plane alignment and co-rotation is not a generic prediction of ΛCDM, and in fact is a quite rare occurrence in numerical simulations. This tension is particularly problematic for ΛCDM as neither subtle changes to the nature of DM, nor varied assumptions about baryonic physics associated with galaxy formation can solve this problem.

If the DM in our Universe deviates from the *cold* and *collisionless* model that is standard in ΛCDM, then there are further tests yet to be forged owing to observational limitations. For example, since the abundance of very low mass galaxies is highly suppressed in Warm Dark Matter (WDM) and fuzzy DM cosmologies, the satellite mass functions, satellite merger rates, and prevalence of stellar streams (which themselves are markers of recent mergers) around dwarf galaxies would all be greatly suppressed. Indeed, both field and satellite dwarf galaxies have been suggested as targets for identifying populations of ultra-low-mass dwarf galaxies (Sales et al., 2013; Wheeler et al., 2015). Additionally, the observation of the intra-halo light (IHL), that is expected to be dominated by stars tidally stripped from galaxy mergers, will test whether or not IHL is the main contribution to the excess of infrared fluctuation observed when cosmic background is subtracted in deep Spitzer data (Kashlinsi et al. 2005). *Such tests have not yet been extensively carried out because of the requirements: wide field-of-view survey imaging down to ultra-low surface brightness limits.*

At the heart of our quest to probe the ΛCDM model tensions falls a need for deep imaging on a large sample of nearby galaxies, specifically extending into the ultra-low SB regime. For example, while the existence of satellite planes or the too-big-to-fail problems may challenge the ΛCDM model, these tensions have only been investigated in detail in the Milky Way (MW) and M31. To test the ΛCDM model, we need to measure the luminosity functions (LFs) of satellite galaxies around nearby galaxies. We also need to better understand the prevalence of systems that appear to have satellite galaxies arranged in planar configurations. Finally, we need to identify which systems possess stellar streams, determine their frequency, and statistically characterize the shapes and abundances of those features. The **"Analysis of Resolved Remnants of Accreted galaxies as a Key Instrument for Halo Surveys"** (ARRAKIHS) mission is designed to address these outstanding needs.

Over the last decade, several ground-based surveys have started to explore the ultra-low SB universe. However, the deepest observations to date, using a variety of small and large ground-based telescopes, typically reach SB levels of "only" ∼28 mag/arcsec^2 in visible wavelengths (VIS), with just a handful of galaxies being observed down to 29 mag/arcsec^2 (e.g. Mihos et al., 2013; Abraham & van Dokkum, 2014; Duc et al., 2015; Martínez-Delgado et al., 2010, 2015)[1]. Imaging to SB beyond 28 mag/arcsec^2 in VIS from the ground has proven indeed very challenging. The major obstacle is the sky background, typically 21.8 mag/arcsec^2 in V-band. This obstacle becomes almost insurmountable at infrared wavelengths (NIR) where the sky background is ∼250 times brighter (i.e., 14.4 mag/arcsec^2 in H-band in the best astronomical sites). To reach SB > 28 mag/arcsec^2 in survey mode from the ground, as needed to resolve the tensions in the ΛCDM model described above, is simply not feasible at this time.

Instead of using ground-based telescopes, the exploration of the ultra-low SB universe can be most efficiently done using small telescopes with large field of view (FOV) on-board a small satellite above the Earth's atmosphere. This is precisely the rationale behind the ARRAKIHS mission.

The *ARRAKIHS* satellite is equipped with two wide-field binocular cameras that will systematically observe the stellar components for 50 nearby galaxy halos per year from space down to an unparalleled ultra-low SB=31 mag/arcsec^2, simultaneously at Blue (HST-F475X) and Visible (Euclid-VIS) wavelengths and down to SB=30 mag/arcsec^2 in NIR wavelengths (Euclid Y and J). These observations will be at least 1.5-2 mag/arcsec^2 deeper than those in the *Euclid* Wide Survey (Euclid Collaboration et al., 2022). Although comparable in depth to the *Euclid* Deep Survey, *ARRAKIHS* will cover a larger survey area and target exclusively nearby galaxies. With 1.4 degree FOV, the *ARRAKIHS* cameras will image the entire galaxy halo in a single pointing with spatial resolutions of 0.8 arcsec in VIS and 1.25 arcsec in J, respectively. These observations will offer a unique view into the still largely unexplored ultra-low SB universe, and provide the key data needed to test the following outstanding challenges for the CDM model.

3.2 Scientific Objectives

The *ARRAKIHS* mission will test predictions of ΛCDM by observing a volume-limited and flux-limited sample of nearby MW-galaxy haloes down to ultra-low surface brightness at visible and infrared wavelengths. The *ARRAKIHS* mission will specifically: (i) characterize the abundance and locations of satellite galaxies, down to $M_V < -6$ for a complete sample of MW-like galaxies beyond the Local Group; (ii) provide robust statistics of the numbers and shapes of wide and thin stellar streams; and (iii) characterize the shape and extent of the ultra-faint IHL. The background, observational/technical requirements, and anticipated results for each of these study areas is outlined below.

3.2.1 Science Case A: Satellite galaxies beyond the Local Group.

CDM model simulations predict a much greater number of dwarf-galaxy size sub-halos embedded in larger galaxy halos than what is actually observed. This discrepancy is observed for the Local Group, which is the best studied galaxy system (e.g. Moore et al., 1999; Klypin et al., 1999), but there are hints that satellites are also under-abundant in nearby galaxies (e.g., Carlin et al., 2019). Similarly, one of the most serious

[1] The analysis of low SB observations has been hindered by the lack of consensus on the most appropriate method for measuring the SB limit of an astronomical image (Mihos et al. 2019). The most widely accepted method is to measure the width of the background noise distribution over pixels for a fixed sky background area (Trujillo 2016). We follow this approach throughout this proposal by quoting SB limits (i.e., residual sky backgrounds) as 3σ of the SB distribution measured over an area of 10 arcsec × 10 arcsec.

potential problems posed for the ΛCDM model is the suggestion that satellite galaxies of the Milky Way and M31 are preferentially aligned in flattened, co-rotating planes (Kroupa et al., 2005). ΛCDM cosmological simulations predict that these planar distributions of sub-halos have less than 0.5% probability of occurring (Pawlowski, 2018). Thus, while the accretion of substructure is a fundamental pillar in ΛCDM galaxy assembly, the observed abundances and distributions of satellite galaxies are in tension with basic ΛCDM predictions.

The baryonic physics that drives galaxy formation has offered a few avenues to reconcile some of the tensions between ΛCDM and observations. For instance, the luminosity function of satellites in the MW or M31 can be in good agreement with ΛCDM expectations by assuming that most subhalos form very few stars (e.g. Wetzel et al., 2016). But a similar reduction of faint satellites may also be expected if those lower mass subhalos are not there to begin with, for example in warm DM models. Unfortunately, with only the MW and M31 systems mapped to the ultrafaint regime it is impossible to discriminate between a) an incomplete understanding of the baryonic physics shaping dwarf galaxies and b) a fundamental challenge to the ΛCDM scenario.

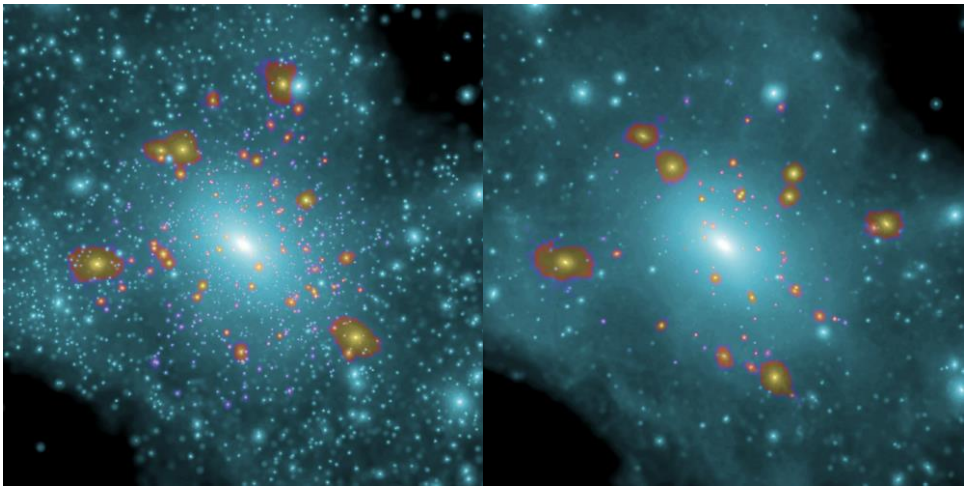

Figure 1: *Projections of the DM distribution in CDM (left) and a WDM model (right) with massive satellites ($M_{stellar}>10^8\ M_\odot$)*

At the heart of these tensions lies a lack of observational data. To test the nature of DM we need a large sample of extragalactic systems analogous to the MW observed with sufficient depth across the virial halo radius to characterize satellite positions and LFs. Such wide field-of-view campaigns have been launched from the ground, but low SB sensitivity is a persistent challenge. For instance, one of the most comprehensive efforts in this line is the SAGA survey (Mao et al., 2021), that has observed 102 MW-like systems (36 of them already published). However, only the brightest satellites can be recovered ($M_r<-12.3$), leaving most of the satellite populations of these hosts below the detection limits. Additionally, the fraction of observed satellites is lower than expected, being this behavior more notorious for low mass satellites (Mao et al., 2021, Fig. 11). Nowadays, it is not yet clear if this discrepancy is just a result of incompleteness in the observational faint end of the luminosity function due to the very low SB>28 mag/arcsec^2 of these satellites, or to a real tension in the CDM model.

Finally, another serious problem posed for the ΛCDM model is the confirmation that satellite galaxies of the Milky Way and M31 have been found to preferentially align in significantly flattened planes, and available velocity measurements are indicative of a preference of satellites in those structures to co-orbit (Kroupa, 2005). ΛCDM simulations, however, predict such anisotropic phase-space distributions of sub-halos have less than 0.5% probability (Pawlowski 2018). In contrast to the other cases mentioned above, the “satellite planes problem” is not much affected by baryonic processes because the distribution of sub-halos on scales of hundreds of kpc is dominated by gravitational effects.

To solve the missing satellites, and the satellite planes problems, it is essential to make a complete catalog of ultra-low surface brightness satellite galaxies below 28 mag/arcsec^2 for a statistically representative sample of galaxy halos. The accurate photometry of these extremely low SB systems provided by *ARRAKIHS* in the visible and infrared bands is crucial to obtain the stellar masses and metallicities of the detected dwarf satellites, a fundamental step to confirm if their dwarf galaxy nature and to understand their star formation history, including the quenched fraction of satellites around the host galaxy. The multi-wavelength observations are also required to distinguish the faint, unresolved satellites population from the cosmological background. This catalog will allow us to assess whether the predictions of ΛCDM are correct or if they have to be reviewed in favor of other dark matter model candidates, such as Warm Dark Matter (WDM) or Self-Interacting Dark Matter (SIDM), which predict less numbers of dwarf-galaxy satellites (Bose et al 2006; Tulin & Yu 2018).

3.2.1.1 Requirements for Satellite galaxies beyond the Local Group.

We will use ultra-faint imaging of a sample of galaxies to detect their satellite galaxy populations and statistically constrain their LFs. We will select our priority galactic targets to be MW-like mass systems (10^{10} < M_*/M_{sun}< 5 × 10^{10}) from the SAGA survey (Mao et al., 2021) at distances 25 Mpc < d < 40 Mpc. We base our requirements for detecting satellite galaxies on the deep PAndAs survey (Martin et al., 2016) which detected 23 dwarf galaxies around M31. Our science objective is to characterize the LF down to at least the same depth as PAndAs for a representative sample of galaxies beyond the local group. The detected PAndAs systems had visual absolute magnitudes in the range -12<M_V<-6, half-mass radii in the range 0.12<r_h/kpc<3, and V-band central surface brightnesses in the range 25<μ_0/mag/arcsec^2<29.3. Projecting these systems out to a distance of 25 Mpc (assuming exponential surface density profiles) yields 25.7 <μ_e/mag/arcsec^2<30. We adopt the strictest of these surface brightnesses as the technical requirements for studying satellite galaxy properties. Establishing a surface brightness limit in the NIR bands cannot be done as easily empirically since there are no similar observations. We therefore rely on visible bands for satellite detection, and require infrared surface brightness limits of 29 mag/arcsec^2 for color information to discriminate the satellites against background and foreground objects using color-color diagrams. Additionally, the stellar masses of the satellite dwarfs can be estimated using multi-wavelength observations and the relation between the M_*/L ratios and the satellite colors. The degeneracy in the stellar mass estimation that appears in some correlations between the M_*/L ratios and the color index can be broken when various colors are used (e.g. Courteau et al., 2014).

3.2.1.2 Anticipated Results for Satellite Galaxies beyond the Local Group.

A core result from the *ARRAKIHS* mission image analysis is a catalog of candidate satellite positions along with visible and infrared luminosities in four bands: F475X, Euclid VIS, Y and J. With these catalogs in hand, we will create (i) galaxy satellite LFs for all *ARRAKIHS* observed galaxies (ii) average satellite LFs calculated as a function of central galaxy mass (along with well-defined error bars determined via bootstrap analysis), and (iii) well defined estimates of the intrinsic variance in the satellite LFs and dependencies on the environment of the hosts. Given that, at present, satellite LFs are only well defined down to $M_V \approx -8$ for the MW and M31 (e.g. Crnojević et al., 2019), this information alone would represent a major improvement in our understanding of the abundance and variability in satellite galaxy populations.
Additionally, it will allow us to place the satellite populations of the MW and M31 within the cosmological context and determine if the tensions with CDM due to their satellite populations are confirmed or not with a representative sample of the general galaxy population.

The catalog of identified satellites will also enable study of the presence of satellite planes in other galaxies. If satellite planes are a common occurrence in the Universe, then we expect a subset of *ARRAKIHS* galaxies to present with edge on configurations. We will use a combination of cosmological numerical simulations

(N-body and hydrodynamical runs) as well as idealized models to quantify the statistical presence of these planes once projection effects and limited number of tracers are taken into account.

3.2.2 Science Case B: Measuring the statistics and shapes of the stellar streams.

ΛCDM predicts that galactic halos should contain a wide variety of stellar structures: satellites, stellar streams, debris flow, and fully phase mixed structures (see, e.g., Helmi, 2020, for a review). Streams are elongated stellar structures, with or without a progenitor present, that are currently being disrupted due to the gradient of the gravitational potential. These structures can be the remnants of disrupted accreted satellites, which are large and contain multiple stellar populations, or those of globular clusters (GC), which are thin and cold.

The detection and characterization of these faint tidal remnants – including measurements of their abundance, width, and shapes/morphology – probe the recent merger activity, abundance of substructure, shape of the potential, the interaction of the streams with dark substructure (Johnston et al., 1999; Sanderson et al., 2015; Bovy et al., 2016), and even the nature of dark matter, as WDM models predict fewer such structures than CDM models (Viel et al., 2013). At present, leading theoretical models (e.g., the FIRE simulations) develop a population of stellar streams that are at odds with those observed in the MW (see, e.g., Li et al., 2021; Panithanpaisal et al., 2021). The question that arises is then: *are the discrepancies between observed streams and ΛCDM models the result of incompleteness in observing the faint end of the luminosity function due to their very low (>28 mag / arcsec^2) or a real tension in the CDM model?*

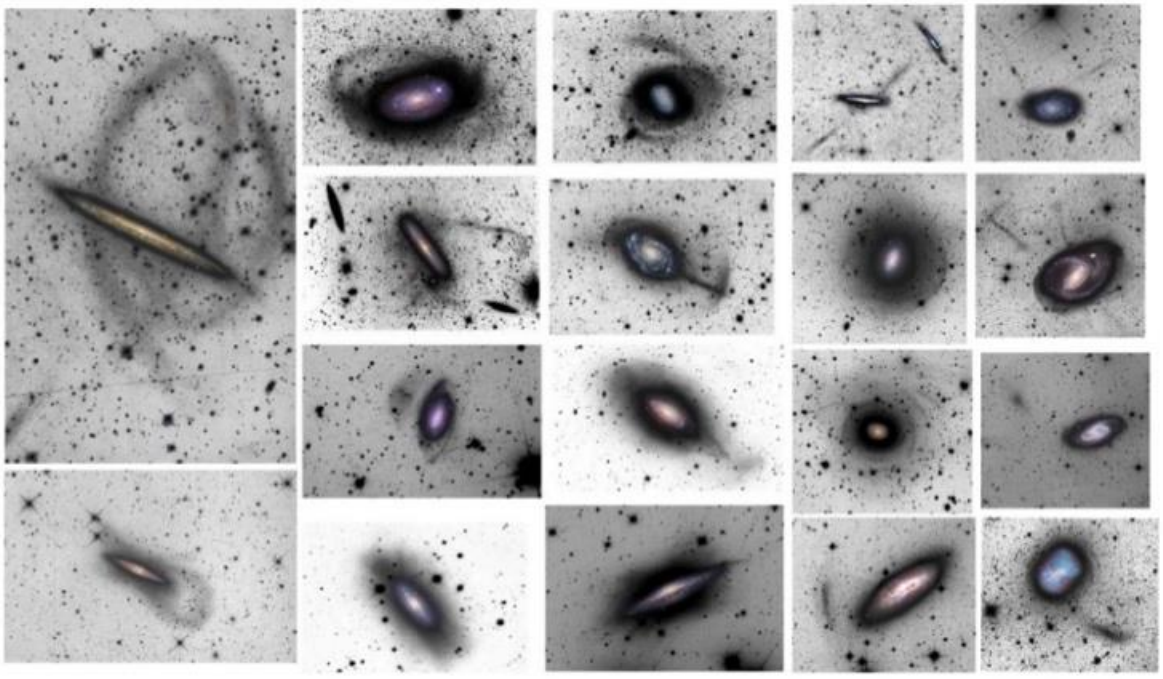

Figure 2: *Luminance filter images of nearby galaxies from the Stellar Tidal Stream Survey showing large, diffuse light structures in their outskirts (Martínez-Delgado et al., 2010, 2012, 2015)*

Although observational examples of the abundance and variety of accreted substructure (Fig. 2) have been discovered around external galaxies (e.g. Cen A: Crnojević et al. 2016, the Stellar Stream Legacy Survey: Martínez-Delgado et al. 2010, 2012, 2015), very-deep ground-based imaging, limited by the atmosphere airglow brightness, have only allowed the detection of the brightest streams (if any) in a handful of galaxy halos after 15 years of observations. The vast majority of large-scale tidal structures predicted in the simulations are fainter, with typical SB > 29 mag/arcsec^2 (Figure 3). A large, unbiased sample of tidal structures observed down to SB =31.0 mag/arcsec^2 is essential to make robust statistical inferences that

can test the predictions from cosmological and galaxy formation theories. The unique combination of ultra-deep visible and infrared images will also allow us to characterize the physical properties of these halo stellar populations, including their ages and masses.

In addition to the number of stellar streams, the CDM model predicts that there may exist a number of low mass sub-halos that do not have stars because star formation inside them was suppressed by UV photoionization or by supernova (SN) driven winds (Dekel & Silk 1986). If they do exist, these dark sub-halos may only be detected from the gaps in the stellar streams they would create due to gravitational interaction, or from the broadening of these streams due to kinetic heating (Yoon, Johnston & Hogg 2011). As explained above, the GC stellar streams are narrower and fainter than dwarf galaxy stellar stream, hindering the detection. However, as the stellar population of GCs is old and metal-poor, NIR observations will favor the detection of such structures as they will be brighter in the IR. Alternatively, a lack of dark sub-halos would result in thinner and unperturbed streams. The shape of these stellar streams in a statistically representative sample of galaxy halos thus provides additional evidence to support or deny another key prediction of the CDM model.

ARRAKIHS will provide the first comprehensive survey of a large population of wide accreted streams and, potentially, thin GC stellar streams. This unparalleled survey of stellar streams will not only benefit from a ×4 larger galaxy sample than ground-based surveys, but also from reaching ×10 deeper in surface brightness. This will specifically enable for the first time a statistical analysis of stream populations in multiple systems.

By characterizing stellar streams in multiple galactic halos, we can (i) learn about the recent merger history, and (ii) probe the disruption mechanism which is a product of the merger orbit and DM halo (which are both predictions of our adopted cosmology and DM model). Alternatively, identifying large populations of galaxies lacking streams all-together would pose a serious challenge to ΛCDM.

3.2.2.1 Requirements for stellar streams.

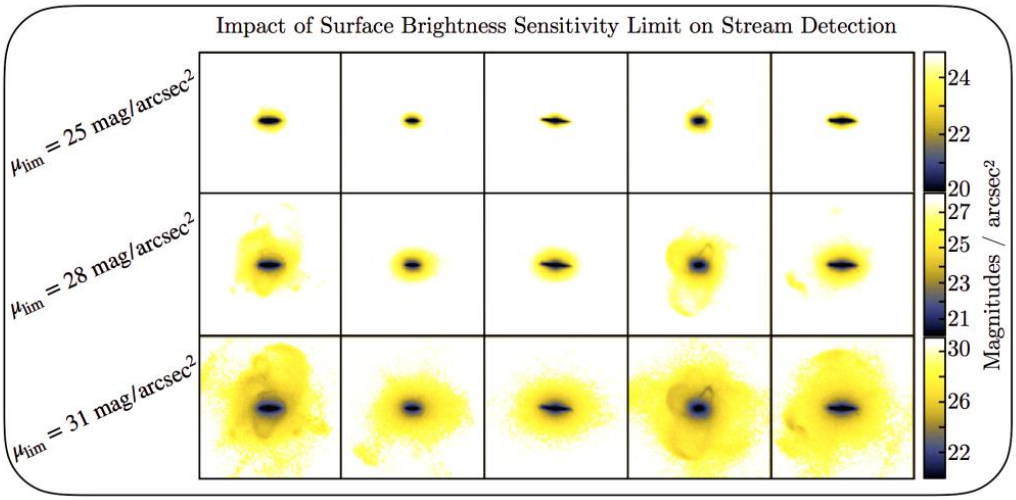

Figure 3: *Mock surface brightness maps from the Aquarius simulations down to varied surface brightness limits from the Auriga simulations (Grand et al., 2017; Vera-Casanova et al., 2021)*

To set the technical requirements for the detection of thin stellar streams, we adopt the methodology of Pearson et al. (2019). We calculate the surface brightness of a stream with the same width, length, and mass as Pal-5, with an age of 3 Gyr and metallicity of [Fe/H]= −0.5. Such objects will be as bright as μ = 28.9 mag/arcsec^2 in the Euclid J-band. While such young streams do not have as long time to form as Pal 5, it is

plausible that streams from such GCs exist in external galaxies. Thus, we adopt a J-band surface brightness detection limit of 29 mag/arcsec^2

The abundance of accreted galaxy stellar streams at very low surface brightness's is not well empirically constrained. To set the requirements, we therefore assume a Schechter luminosity function for the number density of galaxies (e.g., Baldry et al., 2008), and assume that the distribution of wide stellar stream surface brightness's would similarly follow a Schechter function. If the current ground-based observable surface brightness limit of 28.5 mag/arcsec^2 in VIS results in between one and a few streams being observable, then an increase in sensitivity to 30.5 mag/arcsec^2 implies a factor of roughly 20 more observable stellar streams from satellite disruption events (assuming current limits are just probing the surface brightness limit where one stream is observable per halo). This is supported by numerical simulations: Figure 3 demonstrates the potential increase in observed features using mock observations derived from the Auriga Simulations (Grand et al., 2017). A limiting surface brightness of 30.5 mag/arcsec^2 means that almost every galactic massive halo should have an observable tidal stream, and most systems will have multiple streams, in line with predictions of simulations (Vera-Casanova et al., 2021). Thus, we adopt 30.5 mag/arcsec^2 as our technical requirement for detection of sufficient number of accreted stellar streams to be able to characterize their frequency and abundance.

The camera field of view must encompass the Virial radius of our targeted systems to observe all possible stellar streams. A system with a Virial radius of 300 kpc located at a distance of 25 Mpc will subtend 1.35 degrees on the sky. Thus, we adopt this minimum imaging FoV as a requirement.

The most demanding requirement for spatial resolution is set by the observations of thin GC stellar streams in external galaxies. We adopt the methodology of Pearson et al. (2019) and assume a stellar stream formed by a completely disrupted GC, as Pal5, with an age of 3 Gyr, metallicity of [Fe/H]=-0.5 and typical size of the GC stellar streams of the MW, that is, 10-20 kpc length and 0.1-0.2 kpc width (see, for example, Pearson et al. 2019 or de Boer et al. 2018), the SB of the stellar stream will be ~29 mag/arcsec^2. The width of these streams translates to min/max angular sizes of 1.3 and 0.8 arcsec for galaxies at our target distance between 25 and 40 Mpc, respectively. The detection of faint objects is optimized when their angular size is comparable to the camera angular resolution. Although 1 arcsec resolution would be then ideal for thin streams, reaching this value in infrared bands, where the old stellar populations of the GCs are brighter, is very challenging for a small telescope aperture. However, wide streams are estimated to be at least twice as wide (i.e., ∼320pc, or 2.6 arcsec). Thus, we adopt a minimum angular resolution scale of 2.6 arcsec in the infrared bands.

3.2.2.2 Anticipated Results for the Statistics and Shapes of stellar Streams.

We will produce comparisons between observed number of stellar streams around massive galaxies to expectations from cosmological simulations for both accreted and GC streams. With a statistical sample of streams, we can investigate stream morphologies and compare to theoretical expectations for accretion histories of various galaxies (e.g., Hendel et al., 2019). Thin, long GC streams can only exist on regular or resonant orbits (Pearson et al., 2015; Yavetz et al., 2021), and we can therefore use their morphology and locations alone to constrain plausible potentials. Comparisons between halo shapes for dwarfs and massive galaxies will be a valuable test of ΛCDM. In the case of multiple detections of thin streams in one galaxy, we can combine the information of several stream to find the most likely DM potential of the hosts (Bonaca & Hogg, 2018). Additionally, we can compare the GC stream populations and distributions in external galaxies to the population of ≈50 GC streams in the MW (Mateu, 2017).

Novel machine learning methods will be developed to further identify these streams. We will therefore create interdisciplinary collaborations to work through different methodologies to detect and study stellar streams, for example training neural networks on simulations to identify stellar streams, or image

recognition techniques similar to what has been used in gravitational lensing. A parallel study on the evolution of stellar streams in different DM models, implemented through the alternative DM modules will be conducted, and a comparison study with the population of stellar streams found will help rule out DM models, including CDM.

3.2.3 Stellar Streams as tracers of the Intra-Halo Light (IHL) in the Local Universe

The extragalactic background light (EBL) provides a cumulative map of the total emission from all stars and galaxies across cosmic time. The multi-wavelength study of the diffuse flux not associated with any resolved (i.e. high surface brightness) astronomical source can be used to constrain the integrated emission from the first galaxies during the epoch of reionization. Recent measurements of source-subtracted cosmic infrared background (CIB) fluctuations in deep Spitzer data (Kashlinsky et al. 2005) identified fluctuations that significantly exceed those expected from the known remaining galaxies at scales >20 arcsec (Helgason et al. 2012). The nature of these fluctuations is currently the subject of intensive research (Kashlinsky et al. 2018). Two different interpretations have been discussed in the literature: (a) these fluctuations correspond to the red-shifted emission of the first stars and black holes from the epoch of re-ionization or (b) they are the integrated emission of stars *outside* galaxies at lower redshift. In this latter scenario, this intra-halo light (IHL) is expected to be dominated by stars tidally stripped from galaxies in mergers (Zemcov et al. 2012; Cooray et al. 2012). Thus, the study of stellar tidal streams in the local Universe offers direct, powerful, and almost unique constraints on ab initio cosmological simulations that in turn can provide detailed predictions for the integrated diffuse emission arising from galaxy formation.

Observables including the magnitude and color of the IHL can be computed and used to estimate the low-redshift stellar contribution from that of early sources. This opens the way to the use of the near-infrared window to observe the physical properties of high-redshift sources (first stars and first black holes) that ionized the neutral gas, which maybe inaccessible to resolved observations even with future facilities.

3.2.3.1. Requirements for galaxy halos

The size of the FoV described above (~1.35 degrees) will allow to enclose the entire region where the IHL is significant. Numerical simulations reveal that overall halo emission can be observed if SB≈30.5 mag/arcsec^2 is reached (Grand et al., 2017; Vera-Casanova et al., 2021; see Figure 3). Additionally, as the objective is to evaluate the contribution of the IHL to the infrared background, the selected Euclid Y and J filters are especially relevant to achieve this objective.

3.2.3.2 Anticipated Results for the IHL

The comprehensive study of ultra-low SB stellar streams in the local universe will also provide the observations required to constrain for the first time their overall luminosity contribution to the IHL. The imaging data will offer a unique opportunity to reveal as yet hidden details of galaxy assembly in the local Universe and make meaningful connections to the cosmological studies of the ELB at higher redshift. We will analyze the contribution of stellar streams to the total luminosity of IHL within dark matter halos and how the properties of tidal streams (e.g. surface brightness, morphology, color) are related to the total mass and structure of IHL in their host. These observations will be combined with a timely analysis of new high-resolution cosmological simulations of hierarchical galaxy formation (Gómez-Flechoso et al. 2023, in prep.; Roca-Fábrega et al. 2023, in prep.). These ambitious simulations are designed specifically for direct comparison to the proposed observations. Consequently, this project will provide significantly updated theoretical predictions for the IHL fraction in massive galaxies at low redshift.

The deep observations will account for the nonlinear effects of recent merger events in currently theoretical predictions for diffuse stellar mass fractions in dark matter halos, which are based on analytic

empirical models of NIR background anisotropies (e.g. Purcell et al. 2007) and whether these predictions are in agreement with those from recent high-resolution, N-body cosmological simulations of hierarchical galaxy formation. Another point that can be addressed is the dependency of IHL fraction on halo mass, which could to be really very small (and possibly constant) for halo mass $M < 5 \times 10^{11}$ $M_{\odot}$, as suggested by analytical predictions. Finally, the contribution of the light from tidal stream star around massive galaxies to the larger fluctuations observed in the ELB can be measured.

3.3 Ancillary Science Cases with *ARRAKIHS.*

Having ultra-low surface brightness images of galaxies has potential widespread utility beyond the primary science cases described above. We identify here some of the anticipated ancillary science cases that can be explored using the *ARRAKIHS* imaging dataset without setting additional mission requirements.

Ultra-faint dwarf galaxies. The ultra-low SB limit of *ARRAKIHS* allows to extend the detection limits of satellite to the luminosity regime of the ultra-faint dwarf (UFD) galaxies (fainter than Mv< -7.7; Simon 2019), similar to that obtained through resolved stellar population searches in the Local Group and other nearby galaxies (e.g., Cen A: Pearson et al. 2022). These UFD are considered the best candidates for fossils of the reionization epoch and represent the extreme limits of galaxy formation. Unlike larger systems, they were very sensitive to cosmic reionization, which heated and removed the gas within low-mass halos, quenching the system, completely halting star formation. As such, they are likely to have undergone little to no evolution since the reionization epoch, which is highlighted by their old, extremely metal poor stellar populations. Due to the lack of evolution since the epoch of reionization, UFD galaxies may carry relic signatures of the early universe, providing unique insight into this epoch. One of the most interesting by-products of *ARRAKIHS* is the detection of these systems around a complete sample of host galaxies beyond the Local Group, something that has been only feasible for a handful of galaxies from the ground so far.

Satellite Quenching via colors. Using the four-band detection of satellite galaxies, we can determine satellite galaxy colors as a function of radius from the central system and thereby infer satellite quenched fractions.

Thin Stellar Stream Gaps. Gaps and under-densities in stellar streams can occur if low-mass DM subhalos, which are predicted to exist in CDM models, gravitationally interact with stellar stream stars (see e.g., Price-Whelan & Bonaca, 2018). If large (e.g., 10x Pal 5-like) streams are detected, *ARRAKIHS* may be able to assess whether gaps are present (or not).

GMCs in the LMC. Targeting the Large Magellanic Cloud (LMC) as one survey object will result in the deepest, most comprehensive survey to date of very young, embedded clusters in Giant Molecular Clouds (GMCs) in the LMC. ARRAKIHS can image the 30-Doradus star-forming region and most of the molecular ridge, – which contains more than 30% of the CO mass of the entire LMC (Kutner et al., 1997; Johansson et al., 1998).

Time-domain archival value. The raw archival deep time-domain imaging dataset that will be taken as a part of the ARRAKIHS mission will include repeated 10-minute images of the same targets. While our concept of operations does not anticipate real time data analysis for triggering prompt transient follow-up, our dataset will provide deep archival time-sequenced imaging of the fields around our target galaxies.

The environments of SN remnants. Supernova remnants are prominent galactic environments offering valuable laboratories to investigate astrophysical processes. The study of such environments would greatly benefit of the ultra-deep, wide-field, arc-second scale imaging capability of *ARRAKIHS*. The supernova progenitors are mainly massive stars, that are frequently found in binary systems. When the supernova occurs, the less evolved companion is likely to be kicked leading to a so-called runaway star. Runaways can notably be revealed in the infrared by bow shocks produced by the interaction of the stellar wind that

sweeps the interstellar material. Highly sensitive observations at the arc-second scale will reveal a significant number of bow shock features. This information is of paramount importance to understand the dynamics of massive stars in clusters. Tracking the history of present runaways which were previously part of binary systems whose companion underwent its supernova explosion will greatly benefit of even a few *ARRAKIHS* observations of the MW disk.

Backsplash galaxies. Dwarf galaxies that have reached distances to the main galaxy larger than the virial radius after their first pericenter (i.e., "backsplash galaxies"), have often been observed in simulations (Santos-Santos et al. 2022). The existence of these galaxies is a consequence of the accretion of groups of dwarf galaxies, where some of them lose orbital energy meanwhile others gain it. The wide field-of-view of our sample, reaching distances larger than the virial radius of the main galaxy, will allow to obtain a census of backsplash dwarf satellites thus contributing to understand the assembly processes in the Universe.

3.4 Sample selection

The ARRAKIHS galaxy sample consists of all 115 MW-type galaxies from the Satellites Around Galactic Analogs (SAGA) survey between 25Mpc and 40Mpc (Geha et al. 2017; Mao et al. 2021; Figure 4).

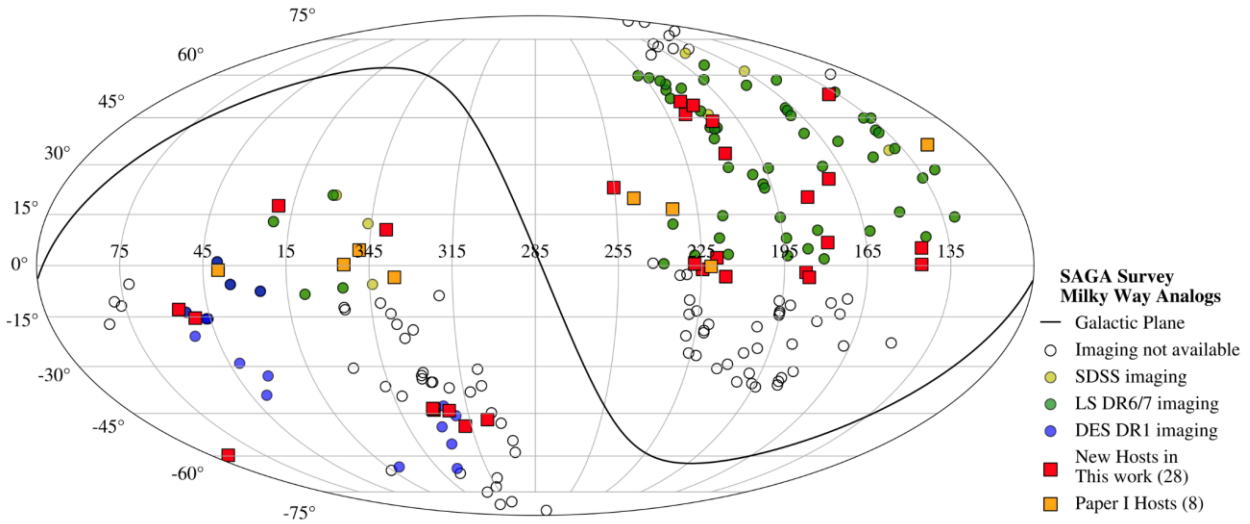

Figure 4: *Sky distribution of 205 MW analog systems identified in the SAGA Survey volume (circles and squares). There are 115 SAGA systems considered for targeting that have complete imaging over at least 99% of the projected virial radius in SDSS (yellow), LS DR6+7 (green), and/or DES DR1 (blue). The solid black line indicates the Galactic plane (Mao et al. 2021).*

Beyond 20 Mpc, dwarf galaxies are increasingly difficult to distinguish from the far more numerous background galaxy population using photometry alone. Actual confirmation of satellite galaxies does require extensive spectroscopic follow-up (e.g., Zaritsky et al. 1997). The SAGA survey will spectroscopically identify satellite galaxies brighter than $M_r = -12.3$ around this volume-limited and mass-limited sample of 115 MW analogs. However, only the brightest satellites can be identified from their observations, leaving most of the host's satellites well below the detection limits.

ARRAKIHS will extend the SAGA survey to explore the dwarf satellite galaxy population of these MW-like analogs down to the same depth of the PAndAs survey (i.e., $M_r = -6$), currently feasible only for the Local Group. Statistical methods have already been used to differentiate the population of satellite galaxies either using magnitude-size diagrams (e.g., Xi et al. 2018) or color-magnitude and color-color diagrams (e.g., Geha et al. 2017). Foreground galaxies pose no major problem since they can be subtracted from the sample based on morphological discrimination, as the size of these foreground galaxies is large enough to be identified and classified morphologically. Contamination by background galaxies pose indeed the main

challenge. The completeness and contamination of the satellite galaxies population in our survey will be addressed in detail during the initial phase of this project, including a thorough examination of traditional discrimination criteria for background sources such as: (i) morphology, (ii) magnitude-size diagrams, (iii) color-color diagrams, and (iv) statistical subtraction of "blank fields" with the same depth of the actual target fields in all four bands. A key advantage of our observational strategy, however, is the large FoV under consideration. At the distance range of our survey, this FoV translates into 1.0 Mpc angular diameter. Since the typical halo virial radius of the halo is 300 kpc, about 85% of the galaxy haloes in our sample occupy just the central 0.55 deg^2 region of our FoV, leaving a ~1 deg^2 region around it to estimate the properties of the background galaxies *within the same region of the Universe as that behind the galaxy halo itself*. A plot of the radial density profile of galaxy counts as a function of the distance to the center of the FoV, should yield a decreasing function up to a given radius where the background galaxy level is reached. Give the large area around the central galaxy halo it is likely this background level can be accurately determined for each one of our galaxies and, therefore, correctly subtracted. In this way, a statistically accurate estimation of the faint-end of the galaxy luminosity function can be obtained.

3.5 Synergies with other ground and space-based observatories

Euclid: Euclid and ARRAKIHS may observe similar areas defined by the avoidance of the strong zodiacal light and the Galactic extinction with the same set of VIS, Y and J filters. However, the Euclid Wide Survey will reach "only" down to SB=29.5 mag arcsec^2 in VIS, and SB=28.4 mag arcsec^2 in J. ARRAKIHS offers a complementary opportunity for observing specific Euclid fields reaching 1.5-2 mag/arcsec^2 fainter than the Euclid Wide Survey, revisiting interesting targets observed by the ESA Flagship observatory, a unique feature of this proposed F-mission. Thus, ARRAKIHS and Euclid are coordinating a strategy for deep follow-up imaging of specific Euclid target fields. In addition, the inclusion of the blue filter in ARRAKIHS offers an enhanced capability to the Euclid observations: while the VIS optical detector of Euclid (5000-9000A) is ideal for the detection of broadband emission from galaxies, this filter is unable to distinguish between old stellar components and relatively younger (bluer) emission from young stars and gas. ARRAKIHS observations will allow to disentangle for the first time the nature of the extended, low surface brightness emission in the outer regions of galaxies, separating ancient stellar halos from the pristine gas inflows from the Cosmic Web.

Ground based observatories: Deep observations down to magnitudes reaching 30 mag/arcsec^2 in visible wavelengths can be achieved from the ground, but only using 10m-class telescopes and only for a small handful of galaxies (e.g., Trujillo et al. 2016). In practice, a general facility observatory like GTC or Subaru cannot possibly be used for a ~100 deg^2 survey of the ultra-low SB universe as proposed in ARRAKIHS. The amount of time and cost required to complete such survey even using world-class astronomical facilities would make it simply unfeasible in visible wavelengths and downright impossible in the infrared from the ground. Even the Rubin observatory, the ground facility par excellence for wide area surveys, will take ten years to reach depths similar to that of the Euclid Wide field in visible wavelengths (Rubin does not have NIR capabilities). An additional advantage of the observations from space is to allow for an enhanced control of straylight that is extremely complicated from the ground, due to the high number density and morphological complexity of sources (Borlaff et al. 2022). Straylight is the second major contributor to the sky background, just below the zodiacal light, and it is responsible for a great number of parasitic gradients that limit the capability to detect large-scale, ultra-low SB features. With ARRAKIHS vantage position in LEO, correction of straylight to the required levels is possible without the risk of fitting and over-subtracting the sources of interest.

Considering the complementarity between the Euclid and Rubin observatories, the ARRAKIHS consortium has already agreed to dedicate up to 20% of the total observing time to projects in collaboration with the astronomical community at large interested in the exploration of the ultra-low SB universe in coordination with the Euclid and Rubin observatories.

4 SCIENTIFIC REQUIREMENTS

4.1 Top level scientific requirements

The scientific performance requirements for the payload are summarized in the table below.

Science Traceability Matrix

Science Objetive	Observation approach	Mission Top Level Requirements
Science Case A: Satellite Galaxies a) Identify satellites throughout the viral radius of a sample of nearby galaxies. b) Tabulate the average luminosity function in F475X and the Euclid VIS, Y and J bands. c) Calculate the variance of individual galaxy luminosity functions. d) Calculate satellite quenched probability using multi-band imaging.	Visible deep imaging	SB > 29 mag / arcsec^2
	Near Infrared deep imaging	SB > 29 mag / arcsec^2
	Satellite counts throughout Virial radius	r_{200} of 300 kpc included in field of view at 25 Mpc (1.35 deg x 1.35 deg)
	Target count	100 galaxies
Science Cases B & C: Stellar Streams a) Identify stellar streams throughout the viral radius of a sample of nearby galaxies. b) Tabulate the average number of thin and thick streams detected. c) Reconstruct their 3D shape to compare against predictions from varied DM models	Visible deep imaging	SB > 29 mag / arcsec^2
	Near Infrared deep imaging	SB > 29 mag / arcsec^2
	Wide/Thin Stream Differentiation	Min spatial resolution of 500 pc at 40 Mpc in J-band (2.6 arcsec)
	Stream counts throughout Virial radius	r_{200} up to 300 kpc included in field of view at 25 Mpc (1.35 deg x 1.35 deg)
	Target count	100 galaxies

4.2 The Case for a Small Space Telescope

As described above, simulations of tidal debris around Milky Way–like galaxies (e.g., Bullock & Johnson 2005; Cooper et al. 2010, 2013, 2017) indicate that the majority of accreted stars reside in tidal streams with SB levels $\gtrsim$29 mag/arcsec^2. To reach such low SB in survey mode is indeed very challenging and requires innovative technological solutions. The rate of photons per pixel (Φ) detected from an object with SB (in AB mag/arcsec^2) can be approximated by the following expression (Abraham & van Dokkum 2014):

$$\Phi \approx \frac{a f^{-2} \bar{E} (3631\ \mathrm{Jy/arcsec^2}) 10^{-0.4\mu}}{h} \left(\frac{\Delta\lambda}{\bar{\lambda}}\right)$$

where a is the pixel area, f is the focal ratio, $\bar{E}$ is the average overall system efficiency, $\Delta\lambda$ is the filter bandpass and λ is the effective wavelength of the filter. As can be easily inferred from this expression, a standard 50mm commercial camera lens with f/2 has the same "light gathering power" as the 10.4m Gran Telescopio Canarias (GTC) with f/16 when expressed as the number of photons per unit detector surface. The difference is that GTC images an area of the sky that is several thousand times smaller. Although GTC has been used to obtain a very deep image of a nearby galaxy (Trujillo & Fliri 2016), these large ground-based observatories are not best suited to carry out a large area survey at very low SB.

Over the last decade, two main approaches have been adopted to optimize the efficiency of surveys aimed at exploring the ultra-deep universe from the ground. Both are based on the use of small telescopes with apertures ranging from 10cm to 80cm. One approach focuses on the development of a system of refractor telephoto lenses (e.g., the so-called "Dragonfly Telephoto Array", Abraham & van Dokkum 2014), with custom software for instrumental control and robotic operation. An alternative approach –and a very successful example of "citizen science" project– consists of coordinating observations taken with high-quality amateur observatories hosting a variety of mostly small reflector telescopes (e.g., the "Stellar Tidal Stream Survey", Martínez-Delgado 2010, 2020; Javanmardi et al. 2017, Figure 5). Their sensitivity, fast operation and lack of competition for observing time typical of professional observatories have placed these low-cost robotic amateur facilities at the front line of ultra-deep imaging and provided major contributions to the research of low SB galactic structure in nearby galaxies.

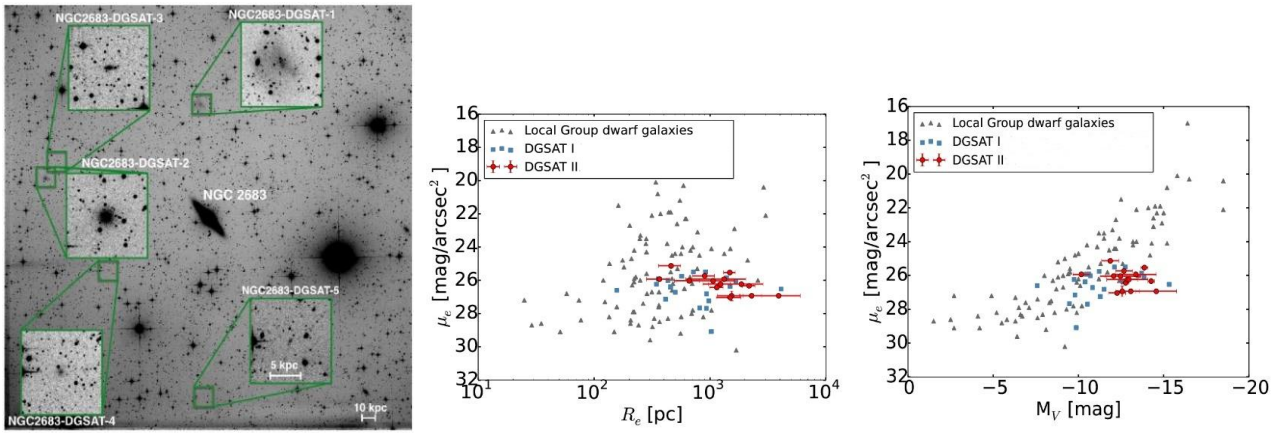

Figure 5: *Faint dwarf galaxies discovered with ground-based amateur telescopes (**left**; Javanmardi et al; Henkel et al. 2017). Comparison of the discovered faint satellites in size (center) and luminosity (**right**) with the Local Group dwarf galaxies.*

However, the deepest observations to date, using a variety of small and large ground-based telescopes, typically reach optical SB levels of "only" ~28 mag/arcsec^2, with just a handful galaxies being observed down to 29 mag/arcsec^2 (e.g., van Dokkum 2005; Tal et al. 2009; Martínez-Delgado et al. 2010; Atkinson et al. 2013; Mihos et al. 2013; Abraham & van Dokkum 2104; Duc et al. 2015; Martínez-Delgado 2020).

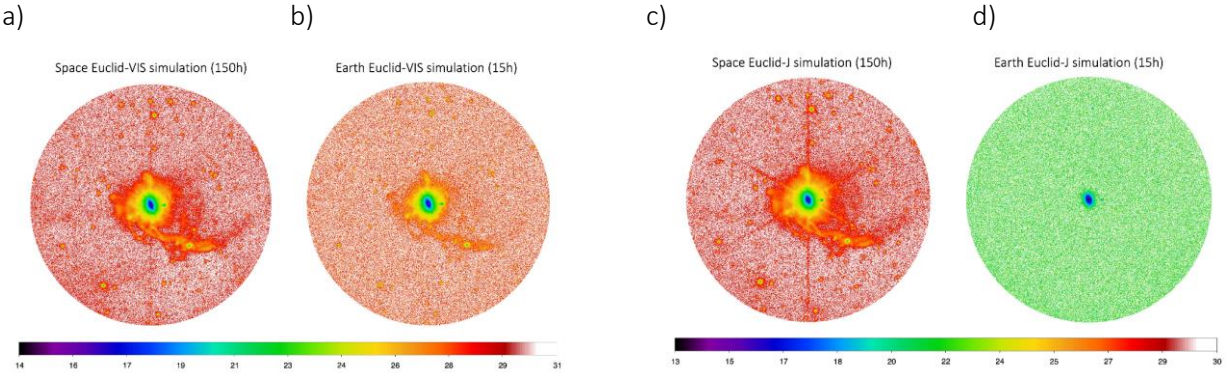

Figure 6: Left*: simulated image of a nearby galaxy halo taken using a small 170mm aperture telescope on board a small satellite in LEO (a) and from the ground (b) in Euclid VIS filter. The SB$_{limit}$ are 31 mag arcsec^{-2} and 28 mag arcsec^{-2}, respectively.* ***Right****: simulated image of the same object with the same telescope from space (c) and from the ground (d) in Euclid J filter. The SB$_{limit}$ are 30 mag arcsec^{-2} and 22 mag arcsec^{-2}, respectively. These observations are representative of the typical exposure times and depths that can be reached from space and from the ground. A detailed information on these simulations is provided in section 5.6.*

Although these ground-based surveys are starting to produce very deep images at optical wavelengths of scores of galaxies, a meaningful comparison between data and models demands very deep imaging data for many galaxies with a simple, quantitative selection function based on a more fundamental quantity,

i.e., *the stellar mass of the host galaxy and the tidal streams*. Since stellar masses require accurate infrared observations, it is thus essential for these surveys to image the universe at very deep SB levels *both in optical and infrared wavelengths.*

Imaging to SB fainter than ∼28-29 mag/arcsec^2 in optical wavelengths has indeed proven very challenging. The first major obstacle to obtain this very deep observations using ground-based telescopes is the sky background, typically 21.8 mag/arcsec^2 at 550 nm. This obstacle becomes almost insurmountable at infrared wavelengths where the sky background can be ~250 times brighter, reaching 14.4 mag/arcsec^2 at 1.5 μm even in the best astronomical sites.

As an alternative approach to using ground-based telescopes, the exploration of the ultra-low SB universe can be very efficiently done using small telescopes (aperture ≳150 mm) with large fields of view (FOV ≳ 1 deg^2) on-board a microsatellite in Low Earth Orbit (LEO). This is the main scientific rationale for the *ARRAKIHS* space mission (see Figure 6).

Finally, the simultaneous observations in four bands provides not only the required dataset to carry out an accurate background subtraction while minimizing contamination and maximizing completeness of the dwarf satellite samples, but also key information to characterize the stellar populations of both satellites and streams, including stellar masses, ages, and metallicities. The four filters selected for the *ARRAKIHS* mission ensure that the age-metallicity degeneracy can be resolved (see Figure. 5)

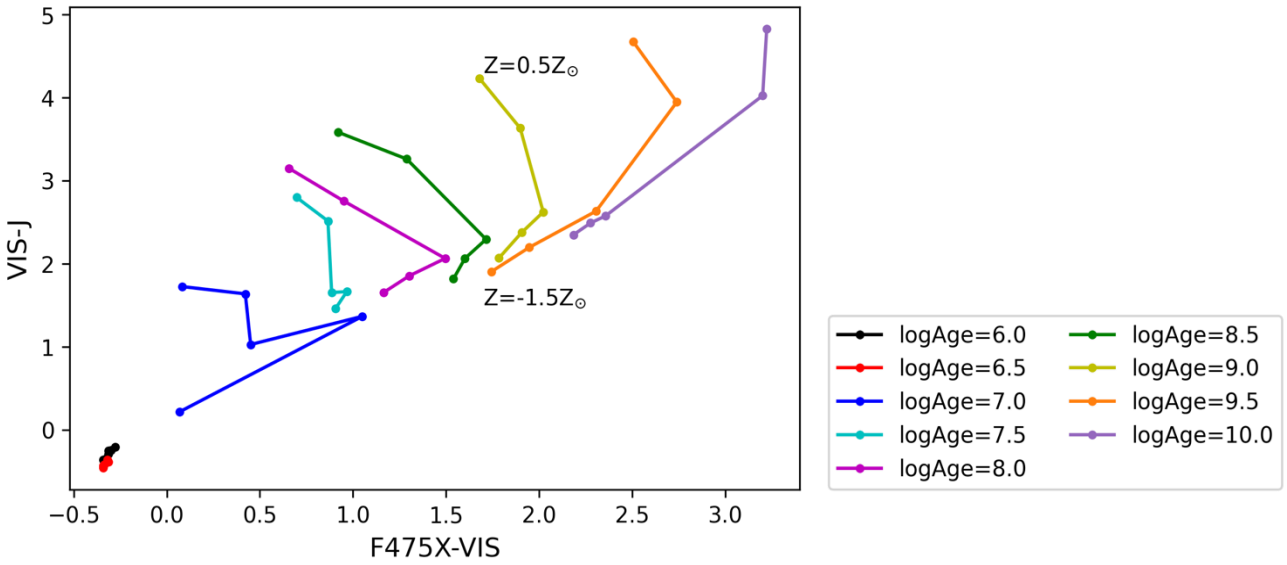

Figure 7: *(F475X-J) vs (VIS-Y) colors for various ages and metallicities proving that the age-metallicity degeneracy can be resolved. We show the combination of Euclid filters that best solves this degeneracy.*

5 PROPOSED SCIENTIFIC INSTRUMENT

5.1 Overview & detection principle

The proposed ARRAKIHS mission payload consists of an **imager** instrument that observes the **visible** and the **near infrared** bands. It is composed by two binocular telescopes, with exquisite optical quality, enabling simultaneous observations in **four bands**. Each binocular has installed two detectors, optimized for the wavelength range, and delivering high throughput and very low noise, required to observe in the low surface brightness regime. The infrared detectors are part of the Fine Guidance System (FGS), that supports the satellite's AOCS accurate tracking with the Payload-in-the-Loop. To perform the scientific measurements down to the required surface brightness, the instrument observes each target in 10-minute exposures, for a total of 150 hours after combining more than 900 exposures per galaxy.

Figure 8: *The ARRAKIHS instrument with two iSIM170 binocular telescopes*

The proposed instrument aims a **simple design**, with no moving parts or filter wheels, with already proven technology and minimized risks.

5.2 Optical System

The following elements were considered in the selection of the optical design:

- Simple optical designs with no moving parts
- Excellent optical performance across the entire FoV with stable and well characterized PSF in the range between 400nm and 1700nm
- Thermally stable system
- Small and light opto-mechanics
- Multi-band capabilities
- Tested and validated in space (TRL > 5)

5.2.1 Opto-Mechanical Design

For the optomechanical design we have identified iSIM, the integrated Standard Imager for Microsatellites, a high-resolution optical telescope developed by SATLANTIS, which has been tailored for small satellites. These characteristics are the result of combining a very compact and straightforward optomechanical design, with the incorporation of advanced manufacturing procedures. In particular, the model iSIM-170, with an effective aperture of 150 mm and a focal length of 1500 mm. On sky, each channel observes a **field of view of 1.4 deg** in diameter.

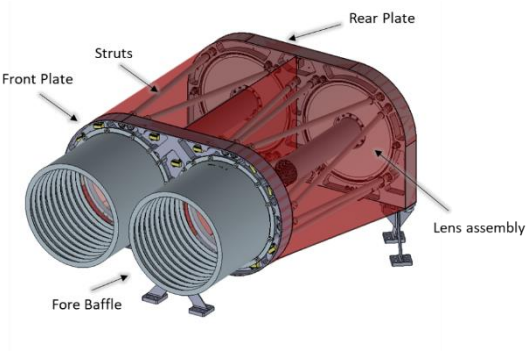

Figure 9: *iSIM170 mechanical configuration.*

The mechanical structure design consists of two plates, a Front Plate and a Rear Plate, connected by 14 struts. The Front and Rear Plates support other elements and assemblies: lens assemblies, filter assemblies, baffles (fore, primary, and secondary), shutter assembly, and detector assembly.

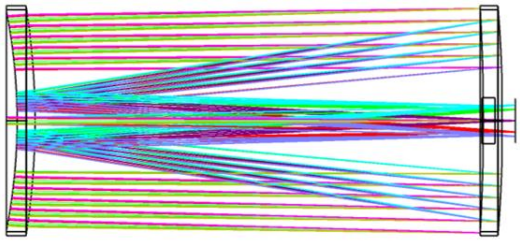

Figure 10: Scheme of the iSIM170 Optical Design

The Optomechanical Subsystem has a binocular design with two optical channels that corresponds to a **modified Maksutov-Cassegrain design** that provides diffraction-limited images for a wide wavelength range (400-1700 nm). Each optical channel is formed by three optical elements and external and internal baffles are included to improve the optical quality by reducing straylight. A Single-Layer Insulation (SLI) is also included internally to isolate the two channels and avoid crosstalk between channels and provide an extra straylight reduction. The mechanical structure design is a high precision, robust and light alloy structure with carbon fibre struts that support the optical system and facilitate the integration and assembly of optical components. With channels dedicated to a specific wavelength range, all optical elements include band-specific high-performance AR coatings that minimize reflections.

5.2.2 Filter System

To achieve the scientific goals, we selected the following filters, each installed in one of the four telescope channels:

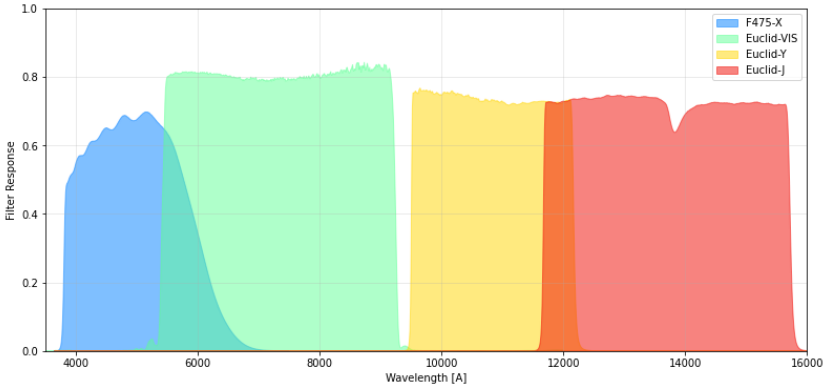

Figure 11: ARRAKIHS filter system.

In the visible channels, we will install the **HST-ACS F475X** (380 to 630nm) filter and a **Euclid VIS**-equivalent band (550 to 900 nm). On the NIR side, we will equip the instrument with **Euclid Y and J** bands (from 945 to 1230nm and 1160 to 1590 nm respectively). The use of Euclid bands enables cross-calibrations between both missions and simplifies additional scientific studies under the same filter system. The bluest F475X band allows to be sky-dominated under all background conditions, and therefore is more adequate than the narrower F475W from the HST system. The four broad bands are shown in Figure 11.

5.2.3 Baffles

The baffling system will be provided from CSL, who has designed and procured the high-performance baffling system for Corot and CHEOPS. In both missions, the strong requirements on straylight rejection (over 10^{13} for field angles above 20 degrees) with a reduced mass suitable for space applications.

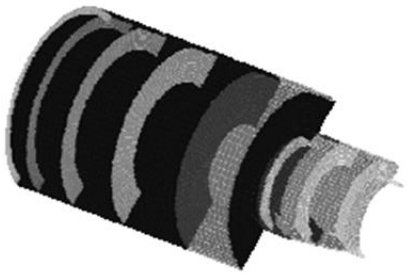

Figure 12: Baffle solution design for strong straylight rejection

When considering the ARRAKIHS payload, the major challenge that will need to be faced is to reduce the straylight to such a level that low-surface brightness targets can be observed. Such a **high-performance baffling** solution will be investigated in Phase A by benefitting from the already derived solutions for the **Corot** and **CHEOPS** space missions.

The first design tasks will consist in down-sizing these baffles to fit with the ARRAKIHS smaller aperture. The positioning of the vanes and internal parts will be optimized through a **detailed straylight analysis** which will eventually testify the fulfilment of scientific requirements.

5.3 Detectors & Front-End electronics

The following elements were considered in the selection of the detectors and front-end electronics:

- High Quantum Efficiency (> 70%) in the target wavelength range
- Low dark current (< 0.5e-/s/pixel) and readout noise (< 5e-)
- High pixel resolution (> 2k x 2k) and small pixel pitch (< 12um and < 20um in the visible and infrared bands respectively)
- Fast read of the full array (< 2 seconds)
- Ability to perform guiding windows in real time for the Fine Guidance System
- Tested and validated in space (TRL > 5)

5.3.1 Visible CCDs

The two bands in the visible range will be observed with CCD detectors. We identified two solutions that meet the specified requirements, one with better performance at TRL4 with a path to TRL5-6 before the mission adoption (CCD250-82) and a TRL8 option with lower performance (less effective FoV and increased pixel size), still non-critical to the success of the scientific goals (CCD273-84).

5.3.1.1 CCD Option A: CCD250-82 & e2v FE electronics

The CCD250-82 from **Teledyne Imaging** is a 4k x 4k 10µm pixel sensor, with 16 amplifiers that delivers an excellent QE over the entire visible range of interest (400-950nm) as seen in figure 17. This detector will be used for the two bands in the visible range (F475X and Euclid VIS). At this pixel size, it delivers a pixel scale of 1.37”/pixel.

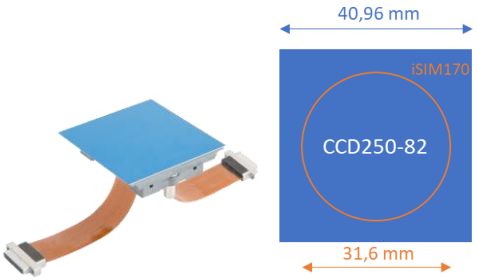

With 16 amplifiers and a readout time of 550 kpix/sec, the entire array can be **read in less than 2 seconds**, rapid enough to minimize the readout trails due to the absence of shutter. The total power dissipation for the CCD250 is 2.4W assuming an image clock speed of 85kHz and a register clock speed of 550kHz.

This detector has **been designed for the Rubin Observatory** and it is currently at TRL4. The packaging would be modified in a configuration suited for space (silicon carbide), as this was designed for a tight focal plane, which is not required in this instrument. The package design would not require mechanical or environmental testing as it has been demonstrated for previous programmes (Euclid & Gaia). A radiation (with proton and gamma irradiation), shock, vibration and endurance campaign would be done before Q3-2024, to quality as **TRL6 before the mission adoption**.

The **front-end readout electronics** design is heavily based on an existing Teledyne e2v CCD front end electronics solution for space and is therefore **already at TRL 5**, subject only to scaling effects.

Wavelengths	400 - 900 nm
Pixel size	10 um
Resolution	4096 x 4004 pix
Dimension	41 x 40 mm
RON	5 e-
DC	0.02 e/s/pix
Operating Temp	178 K
Amps/Freq/T_{read}	16/550k/1.9s

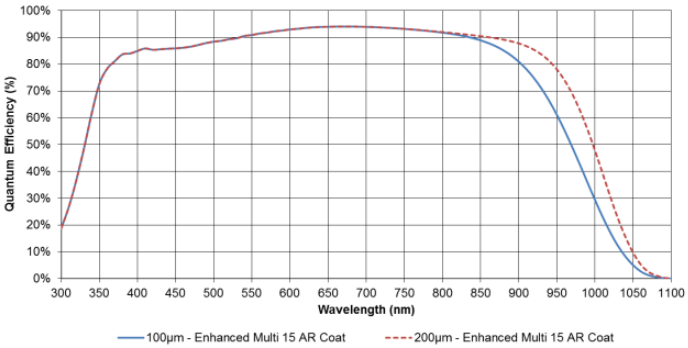

Figure 17: *CCD250-82 quantum efficiency*

Its excellent QE, small pixel size and adequate dimensions with respect to iSIM170 focal plane size, makes this detector an ideal solution to the required sensor needs.

5.3.1.2 CCD Option B: CCD273-84 & MSSL ROE

An alternative solution with **higher TRL** is the CCD273-84, developed specifically for the Euclid VIS instrument. This is a 4k x 4k 12µm pixel detector from Teledyne-e2v technologies. Taking advantage of **Euclid's heritage**, the CCD detectors will naturally incorporate the Read Out Electronics (ROE) from Euclid's VIS instrument (also TRL8). The slightly larger pixel size will deliver a pixel scale of 1.59"/pixel.

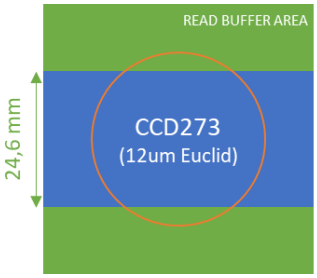

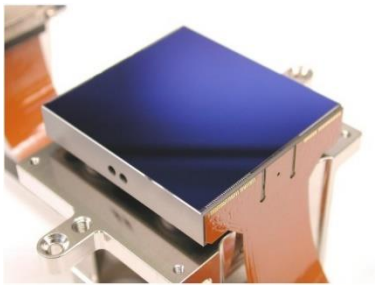

The proposal is to reuse the **MSSL qualified Euclid Readout Electronics** (ROE) (and power supply, RPSU) which provides a space-wire 16-bit digitized output for three CCD273-84. It is potentially possible to use the current design and implementation with only limited changes to service both telescopes with one ROE.

The CCD273-84 is oversized with respect to the iSIM-170 field of view (see diagram above). This detector contains 4 amplifiers and a read frequency of 70 kpix/sec, leading a total readout time of 60 seconds. The readout time would be prohibitive without shutter. However, we can make use of the areas outside the FoV (identified in green) as a **readout buffer**. Charges can be rapidly shifted outside the FoV into the buffer area, and the science image be read at the nominal rate for 30 seconds. A shield over the buffer area made of aluminum and chromium will prevent light entering into the buffer area will deposited into the corresponding area, in a process that Teledyne confirmed is standard and presents no risk.

Wavelengths	400 - 900 nm
Pixel size	12 um
Resolution	4096 x 4096 pix
Dimension	49 x 49 mm
RON	2.3 e-
DC	0.001 e/s/pix
Temp	150 K
Amps/Freq/Tread	4/70k/60s

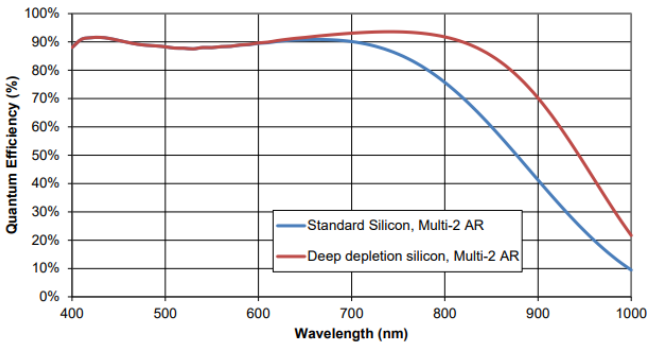

Figure 18: *CCD 273-84 quantum efficiency*

5.3.2 Near Infrared detectors & ASIC

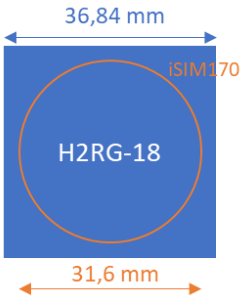

The two infrared bands will incorporate 2x **H2RG** from **Teledyne Imaging** (TRL9), in the configuration with 2k x 2k pixel, 18 µm pitch and 1.75µm wavelength cut-off. The resulting pixel scale will then be 2.3" / pixel. The substrate-removed HgCdTe enhances both J and Y bands QE, above 80%, as shown in Figure 19.

At the operating temperature of 140K, this model delivers a very low dark current performance (≤ 0.5 e-/s/pix). With 32 amplifiers and a readout rate of 100 kpix/sec, the entire array can be read in about 1.5 sec. To reduce the read noise, we will operate the detector in Fowler or up-the-ramp modes, similarly as done in the NISP instrument of Euclid with the same detectors.

The flexible readout system of the H2RG, allows us to read various configurable guiding windows to enable real time centroid corrections to the AOCS (detailed in Fine Guidance System section).

Both science and guiding read modes H2RG will be controlled and acquired with Teldyne's SIDECAR ASIC (TRL9), which enables a reliable and efficient operation and output digitization. A specific space-based configuration of the ASIC will be used for the integrated models, while cryogenic development kits are planned for development and test phases.

Wavelengths	400 - 1600 nm
Pixel size	18 um
Resolution	2048 x 2048 pix
Dimension	36.9 x 36.9 mm
RON	5 e-
DC	0.5 e/s/pix
Temp	140 K
Amps/Freq/T_{read}	32/100k/1.3s

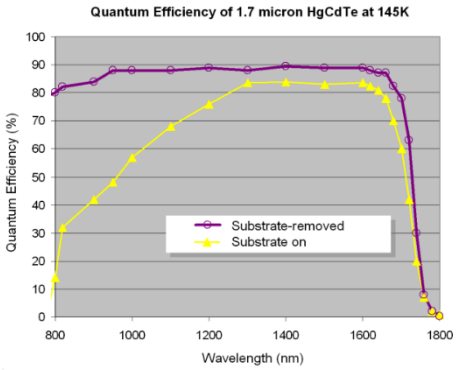

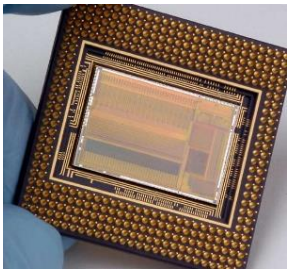

Figure 19: *(**Left**) H2RG quantum efficiency with substrate removed. (**Right**) SIDECAR ASIC*

5.4 Electronics Architecture

Below we detail the electronics system that operates the scientific instrument for both binocular telescopes and the four readout channels. It is composed by two On Board Computers (OBC), each dedicated to one binocular iSIM170 camera and an additional OBC for the Fine Guidance System (FGS) real-time processing. Each VIS and NIR OBC will control the front-end electronics for both detectors and the Thermal Control system, which maintains thermal stability for both opto-mechanics and detectors.

5.4.1 Block Diagram

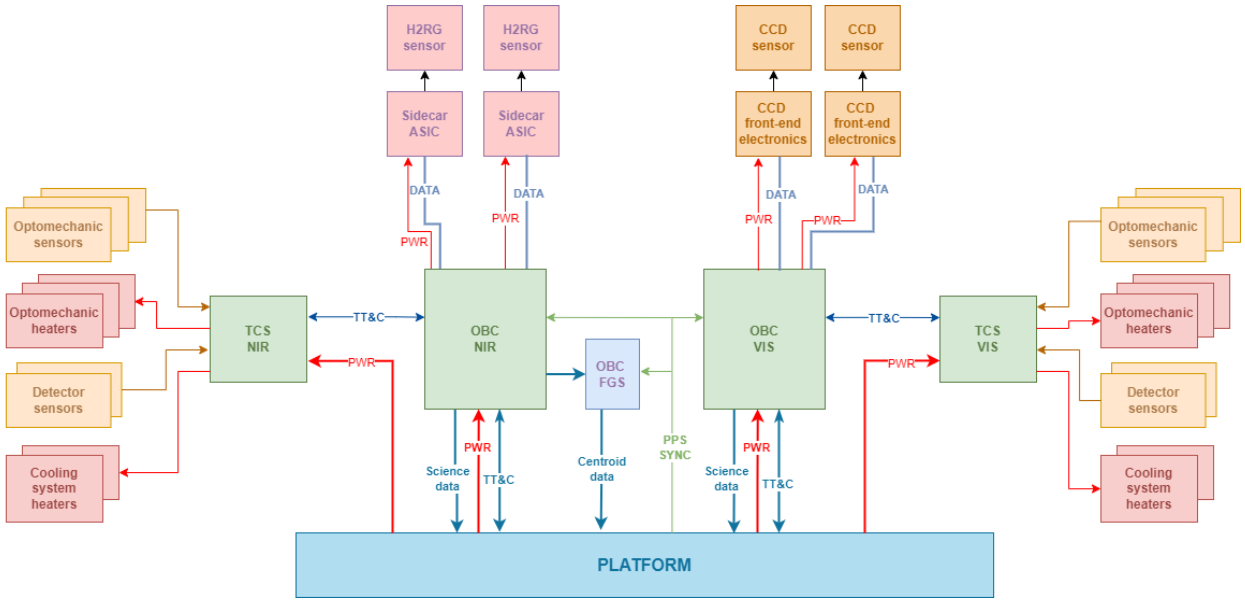

Figure 20: ARRAKIHS electronics block diagram

The electronics include:

- Teledyne's SIDECAR ASIC readout proximity electronics for H2RG sensors and Teledyne's proximity electronics for CCD sensors.
- One OBC for each iSIM170 camera to read science data from 2 detectors each (2 visible CCD and 2 NIR H2RG), send the H2RG centroid data to the FGS electronics and transmit TT&C and science data to the platform. It controls the TCS and per detector.
- One TCS for each iSIM170 to maintain the camera at the desired temperature using thermocouples and heaters. It controls the detector's cooling system heaters (between the detectors and the radiators) and temperature sensors.
- The main power supply for the payload will be directly connected to each OBC and TCS. The corresponding OBC will distribute the power to the detectors.

5.4.2 On Board Computer

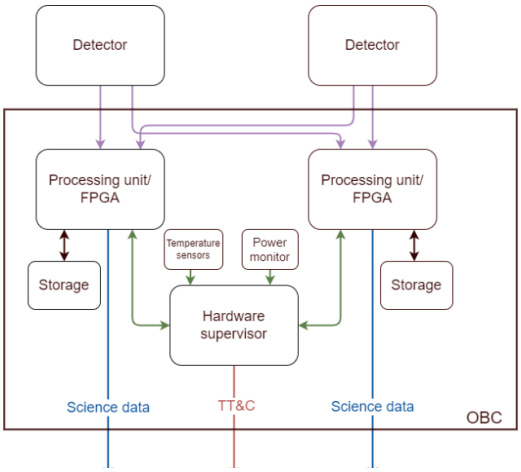

Figure 21: *On Board Computer diagram*

As the on-board computer for the imager SATLANTIS SPoCK board will be used. It has the following main features:

- On orbit reprogrammable
- The hardware supervisor controls the health of the OBC by reading the on-board temperature sensors and the currents and voltages of the main power rails.
- It has two processing units with FPGAs and memories.
- It supports high speed communication with the detectors. The maximum speed needed for the application is 3,2 MB/s.
- It has a capacity of at least 22 GB where approximately 2 days of data can be stored.

5.4.3 Thermal Control System

The Thermal Control System is a separate SATLANTIS electronics board able to control all the heater channels and thermocouple temperature sensors required for keeping the temperature of the opto-mechanics and detectors of the payload within its operational range. It is commanded by the OBC and has reprogrammable capability on orbit.

5.4.4 Fine Guidance System

The scientific requirements of the mission require a precise stability of the **Relative Pointing Error (RPE) below 0.5" RMS** during the nominal exposure time. This ensures that the PSF of the scientific images is not degraded such that it would compromise the final resolution performance. To reach this level of accuracy, we expect that corrections from the payload will have to support the AOCS of the platform during the integration of the science exposures. In this section, we describe the Fine Guidance System (FGS) that enables "payload in the loop" corrections to the spacecraft AOCS system.

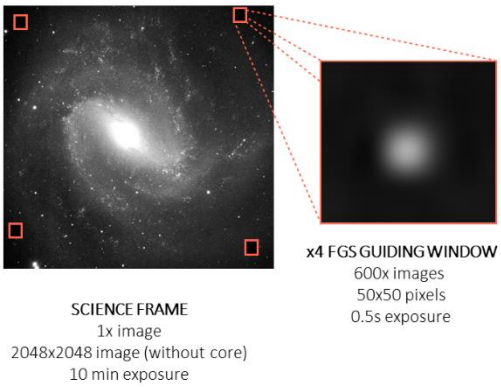

Figure 22: *Fine Guidance System concept*

To achieve this, we make use of the **windowing capabilities of the H2RG**, where we can perform non-destructive reads of the infrared array during the integration time. We will request guiding windows around bright stars in the FoV, where we can measure the centroid and send it to the AOCS with an accuracy better than 0.12" RMS (imposed by the high-performance AOCS study, see section 6.4.2) at a rate of 1Hz.

To ensure we can reach the target centroid accuracy we ran a simulation of the FGS guiding windows, including a realistic PSF in J and Y bands, all H2RG properties (pixel size, dark current, read noise, etc.), a random motion of the AOCS and a representative set of stars (from Gaia) at various galactic latitudes. To provide centroids every second, we consider a guiding window exposure time of 0.5 sec.

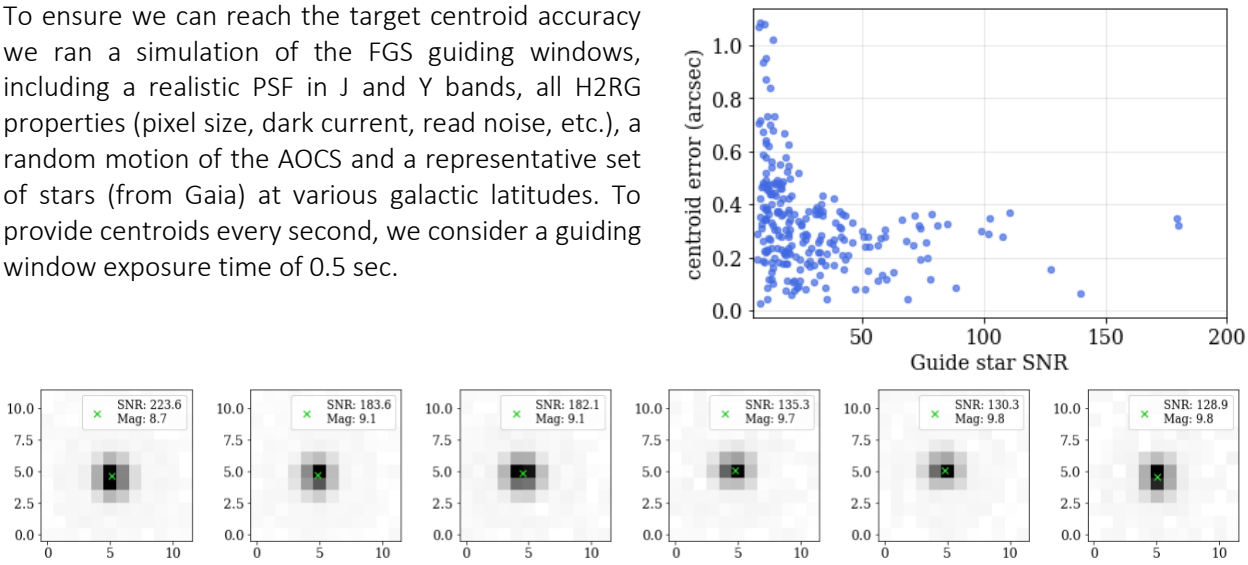

Figure 23: *Fine Guidance System performance study*

The analysis results that both in Y and J band, **we achieve the target 120 milli-arcsec** (mas) precision with **less than 8 guide stars** (with slight degradation in performance in the Y band due to its smaller subsampled PSF). As both infrared channels will be providing guiding windows, we consider four guide stars per channel to achieve the target accuracy.

The University of Vienna, with its expertise in a similar solution adopted for **CHEOPS** and **Ariel**, will provide the real time Guiding software.

5.5 Thermal Architecture

The thermal architecture for ARRAKIHS has been designed by APCO considering the following objectives and requirements:

- The mass of each optical instrument is 15Kg
- The thermal dissipation of each detector is approximately 300 mW
- The thermal dissipation of each electronic unit is 30 W
- Detector temperatures should be within the range of 140K ± 1K with a passive radiator.
- Optical Bench that supports the instruments must be within a temperature range of -20°C ± 5°C

5.5.1 Optical Bench Concept Description

The ARRAKIHS optical bench's concept consists of an assembly of sandwich panels, machined radiators,

thermal hardware and insulation connections, that will provide support and thermal protection to both ARRAKIHS' payloads. The design depicted in Figure 24 has been built around both payloads to fit the satellite envelope and optimize both mass and volume.

The main parts of the optical bench are the following:

- **Detector´s radiator:** A radiator made of a machined plate will be placed above the instruments and connected to the four detectors. The radiator will be machined from milled AA6061 T6 plates. It will be oriented toward cold space so the external fluxes coming from the sun, earth, and albedo are reduced.
- **Heat pipes:** Two heat pipes bent at 90° connect the 4 detectors (two per heat pipe) to the radiator. This design reduces the gradient between the detector and the radiator.
- **Electronics´ radiator:** Two radiators arranged laterally in relation to the instruments are connected to the optical bench. The four electronic units are fixed on these radiators near each instrument. The external face is covered with SSM while the internal face will be coated with either an aluminized SLI or an MLI with an aluminized PET film outer sheet to reduce the radiative flux absorbed by the internal radiator faces.

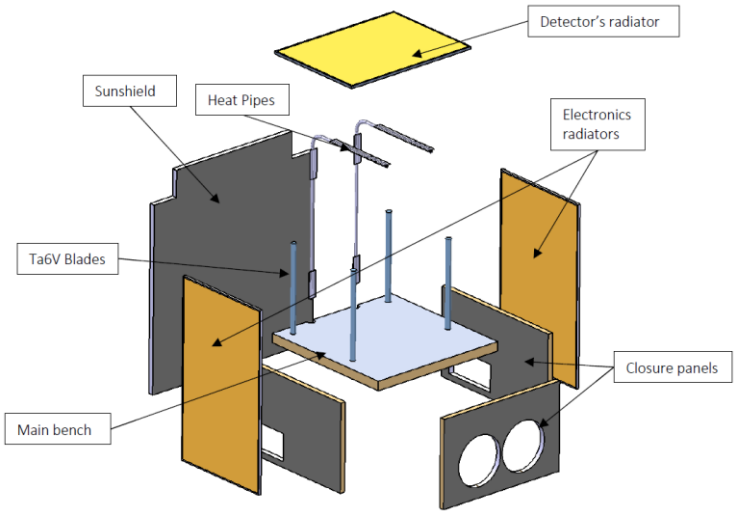

Figure 24: *Optical bench design exploded view*

- **Main bench:** This optical bench supports the two instruments placed one above and the other below. Instrument mounting systems are thermally decoupled. The bench is a sandwich panel made with aluminium skin and an aluminium honeycomb. The skins are covered with Alodine to reduce the radiative exchanges of the optical bench with its environment.
- **Sunshield:** A sunshield is placed on the back of the instruments. This consists of a sandwich panel with a white paint facing the sun and is covered with an MLI with an aluminized PET film on the back (facing the instrument and detector radiators).
- **Titanium blades:** The Supporting parts of the Detector radiator will be machined Ta6V blades, in order to have a low conductance and isolate the radiator from the rest of the structure.
- **Closure panels and MLI blanket** as passive thermal protection: The Supporting parts of the Detector radiator will be machined Ta6V blades, in order to have a low conductance and isolate the radiator from the rest of the structure.

The connections between the panels will be made using cleats that will allow using standard cylindrical cold-bonded inserts. Floating nuts will be mounted on each cleat in order to ease the integration process. All the thermal connections will be insulated by means of thermal washers and other methods that will reduce the conductive coupling between elements.

5.5.2 Thermal Mathematical Model and Preliminary Results

To validate this first concept of thermal control, a thermal model has been developed. The thermal simulations carried out for the preliminary sizing of the thermal control of the ARRAKIHS instruments in a hot winter solstice case (but without tilting) show that the temperature and stability objectives defined in the previous section are achieved since:

- The temperature of the detectors is 144 K (-129°C) with a stability of the order of +/-0.3 K and a maximum gradient between detector < 0.2 K for a specification of 140 K +/- 1K.
- The average temperature of the optical bench is in the range [-23.5°C; -21.7°C] which is compatible with the specification of -20°C +/-5°C.
- The electronic units are within a temperature range of [1°C; 4°C] which is low for a hot case. Reducing the size of the equipment radiator will raise this temperature.

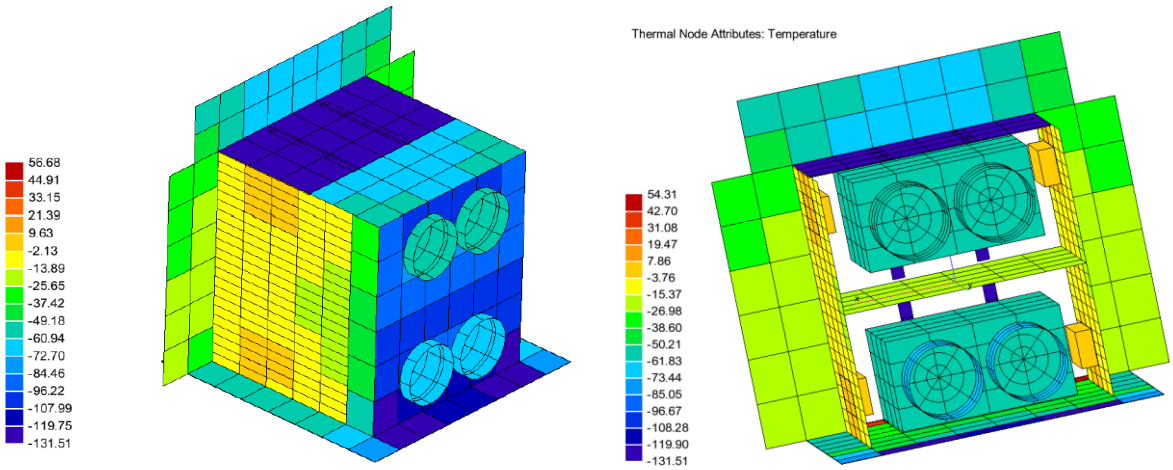

Figure 25: *Temperature mapping of ARRAKIHS thermal design*

5.6 Mass, Power, and Data budget

Below we indicate the expected mass and power budget of the payload and its subsystems. The total mass and power include a 20% margin.

			Units	Weight [Kg]	Average Power [W]	Peak Power [W]
Opto-Mechanical	VIS & NIR	iSIM170	2	24,2	10	80
		Detector Housing	4	2	0	0
		Baffles	4	7	0	0
		Optical Bench	1	8	0	0
		Radiators	3	3,4	0	0
		Heat Pipes	2	0,4	5	20
Electronics System	VIS	OBC	1	1	28	33,2
		TCS	1	0,5	0,5	1
		CCD250-82	2	0,2	0,01	0,1
		CCD ROE	1	2	1,5	4,8
	NIR	OBC	1	1	28	33,2
		TCS	1	0,5	0,5	1
		FGS	1	1	28	33,2
		H2RG	2	0,2	0,01	0,2
		SIDECAR ASIC	2	0,6	0,6	2
			SUM	52,0	102,1	208,7
			+20% Margin	**62,4**	**122,5**	**250,4**

To estimate the total data budget, we include the following considerations:

- VIS detector array: 4096 x 4096 pixels
- NIR detector array: 2048 x 2048 pixels
- VIS & NIR channels: 2 each
- Bits / pixel: 16 bits
- Science & Calibration orbits / day: 13 and 1 respectively
- Number of darks - flats / calibration orbit: 10 and 5 respectively
- Orbit time: 90 min
- Nominal Science exposure time: 10 min
- Bandwidth: 15 Mbit/s
- Compression Factor: 2x

Data / science orbit [GB]	Data / calib. orbit [GB]	Total daily data [GB]	Total daily data compressed [GB]	Transmission /day [min]	Total survey data [TB]
0,8	1,3	11,1	5,5	49,2	16,2

5.7 Instrument Performance Simulations

We have carried out accurate, in-depth simulations of actual ARRAKIHS images including state-of-the art models of galaxy haloes, and a most realistic characterization of the camera performance, and of the actual observational effects from LEO associated to all relevant contaminating sources.

Camera Performance: We have carried out a detailed characterization of the optical properties of the iSIM-170 camera with emphasis on the point spread function (PSF), the light scattering due to inhomogeneities of the optical surfaces and the ghost image analysis, reaching up to 12 orders of magnitude. The polychromatic PSF models are computed in each filter from a set of PSF in 126 wavelengths covering from 300 to 1600nm and considering the diffraction effect produced by the spider that holds the secondary mirror baffle. The camera PSF is convolved with a gaussian of σ = 0.5" considering the micro-vibrations of the platform over the 10-min single exposure. The ghost reflections for point sources and the scattered light due to surface roughness of the iSIM camera, discussed in sections 5.2.4.2 and 5.2.4.3 respectively, are beyond the dominant noise levels for the limiting SB of our observations (or one part in 1 million) so won't have any effect in the final images. However, we can expect a contribution of these ghost reflections because of the galaxy bulge. This effect is stable enough to be modelled and subtracted as has been done for other ground-based refracting telescopes (Martínez-Delgado et al., 2021). The flatfields as well as the detectors noise, including dark current, bias and read-out-noise, have also been simulated following the detectors specifications: CCD250-82 (visible) and Hawaii-2RG (IR). We have also modelled fully the optics and filters throughput in the 4 channels for the iSIM-170 assembly to be used in ARRAKIHS.

Observational effects: The MW-type galaxy model has been provided by GARROTXA (Roca-Fàbrega et al., 2016). We have transformed the numerical mass particle model made with a resolution of 10^3 M_{sun} into luminosities using their metallicity and age for each particle and the corresponding synthetic Color-Magnitude Diagrams (CMD) for the visible and infrared filters mentioned above. To provide a more realistic look to the galaxy image, we apply an adaptative gaussian kernel as a function of the 3D K-Nearest Neighbors (KNN) of the particle distribution. We apply a different 2D Gaussian Kernel with the 3D distance to the 16^{th} nearest neighbor in pixel scale as FWHM for each luminosity particle. We have also simulated all the straylight gradients produced by astronomical objects, including nearby stars (using GAIA catalogue) around the FOV (Fig. 26b), the Earth, Moon, and other Solar System Bodies. We have even reproduced the effect of the orbit which affects to the incident angle of the Earth straylight from exposure to exposure (Fig. 26c). The straylight is calculated applying the so-called Normalized Detector Irradiance (NDI) function that represents the ratio between the energy that comes into the entrance of the camera and the energy that arrives to the detector. The values obtained for this effect are consistent with the results for Euclid mission (~ 26 mag/arcsec^2 in VIS, Borlaff et al., 2022). To calculate the gradients along the detector due to the Zodiacal Light (ZL), we have used the gunagala python package, which mapped the ZL for the entire sky for a given date and wavelength. The ZL is the sky background dominating component, which is also consistent with Euclid results (~ 21-22 mag/arcsec^2, in VIS, Fig. 26d). We have added the Cosmological Background provided by Illustris Project (Torrey et al., 2015, Fig. 26e). The Galactic Extinction is calculated from E(B-V) full-sky maps with a resolution of 6.1' (Schlegel, Finkbeiner & Davis, 1998, Fig. 26f). We include all type stars in the FOV of the camera, using GAIA catalogue for stars with M < 22 and Besançons galaxy model for stars with M>22 (Czekaj et al. 2014, Fig. 26g).

We have simulated a realistic observation sequence, taking 900 10-min exposures along a Low Earth Orbit at 700km of altitude. All observational effects are convolved with the effective PSF of the camera for the

corresponding filter. They are corrected for the total efficiency of the camera (combination of telescope, filters and detector throughputs) and for the flat field of the detector and then, the detector noise is added and all these simulated images are saved to be reduced and processed as a real observation would be. With this same methodology, we simulate a master flat field and master dark images to subtract the detector effects from the already simulated images. Once all the images are processed, we sum the images in 9 groups of 100, in order to create different master sky images for the 9 different incident angle of the Earth straylight which may induce a difference in the sky background. With this master-sky we subtract the sky background for all the images and then, they are all summed to obtain a final image with a total integrated exposure time of 150h. We have used the same procedure for each filter.

With these simulations, we have demonstrated that we can reach a limiting surface brightness of ∼ 31 mag/arcsec^2 in F475X and Euclid VIS filters, and ∼ 30 mag/arcsec^2 in Euclid Y and J filters (3σ, measured over 10x10 arcsec^2). Fig. 27 shows an RGB image with Red = Euclid-J, Green = Euclid-Y and Blue = Euclid-VIS for complete simulation of 150h. We also demonstrate that we will reach a spatial resolution of <1.5" and <2.2" at visible and IR wavelengths.

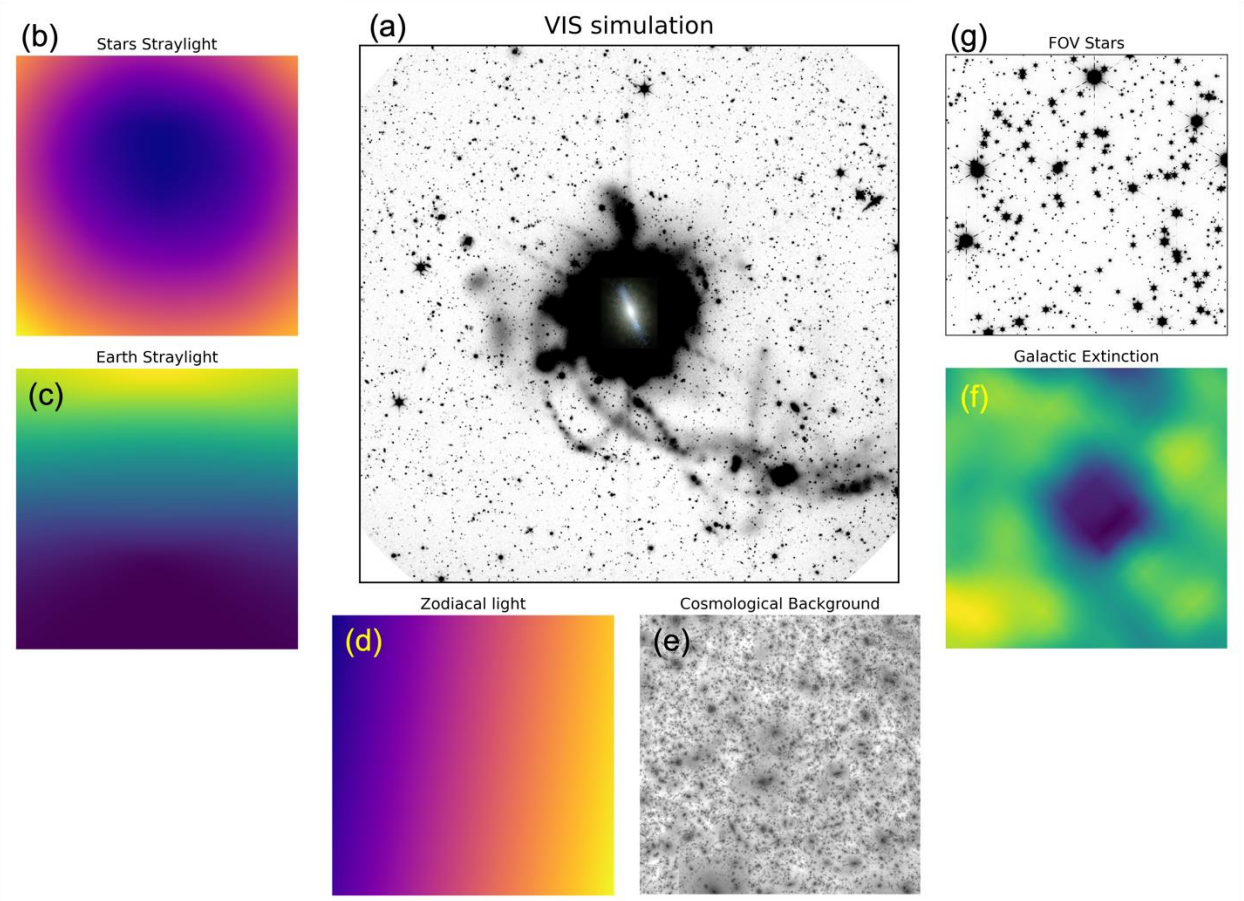

Figure 26: (a) *Result of a simulation in VIS band of a total exposure time of 150h using iSIM-170. (**b**) Straylight coming from all the stars around the FOV of the telescope. (**c**) Straylight coming from the Earth due to its albedo during the exposures (**d**) Incoming Zodiacal light. (**e**) Cosmological background from Illustris Project (**f**) Galactic extinction map from Schlegel et al. (1998). (**g**) Stars within the FOV from GAIA catalogue and the Besançon Galaxy model.*

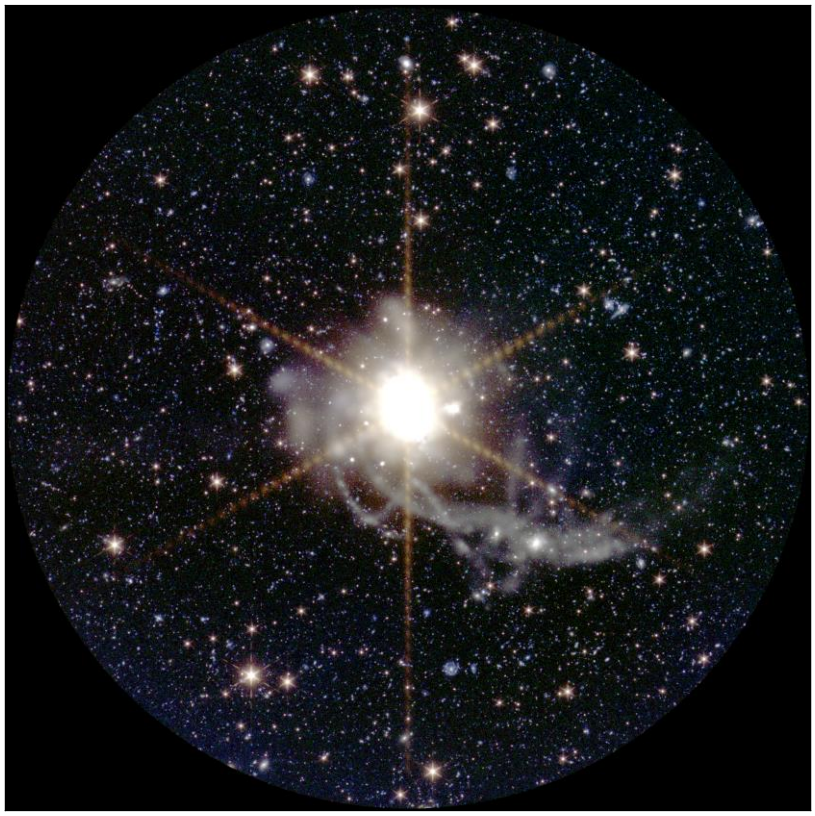

Figure 27: *Composite image of Euclid J(Red), Euclid Y (Green) and Euclid VIS + F475X (Blue)*

To apply the super resolution (SR) algorithms and probe that they can be applied in astronomical observations reaching an improvement in the spatial resolution by a factor of 2. We have computed the same 900 exposures simulations with a non-integer displacement between images. To do that we have sub-sampled the initial images in a 3x3 grid. Now we have repeated the same methodology as explained above, but for each iteration the entire image is displaced and binned to recover the original detector shape. The displacement is calculated from a random normal distribution with a standard deviation of 30". We have computed these simulations for Euclid-VIS and Euclid-J filters to illustrate that we can reach a spatial resolution of 0.8" (Euclid-VIS) and 1.2" (Euclid-J) applying the SR algorithm:

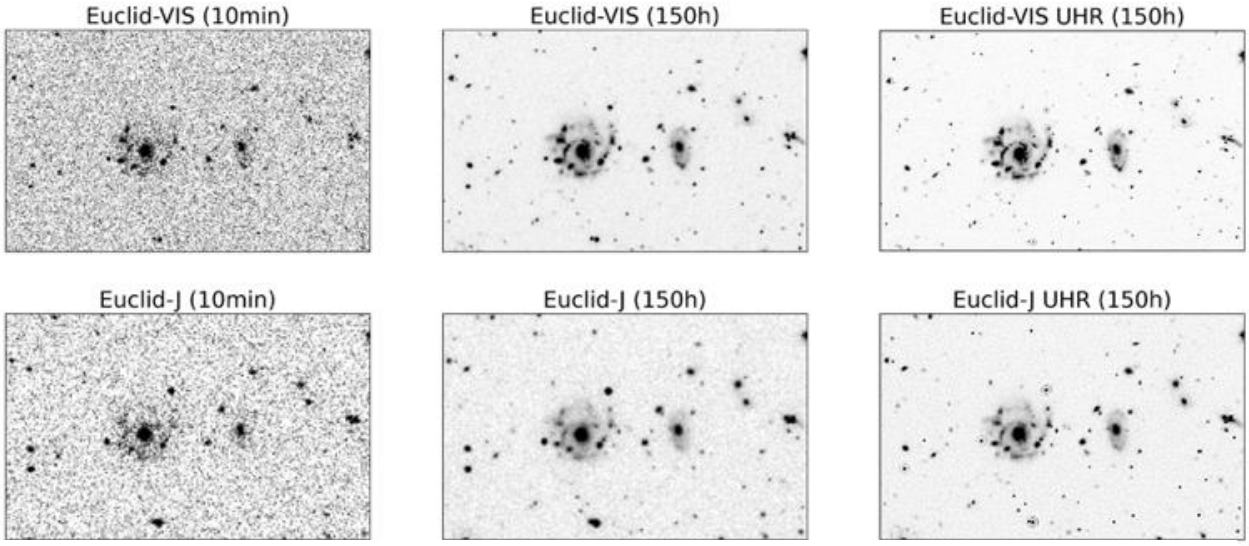

Figure 28: *1st column: single 10 minutes exposure of a cosmological background fields in Euclid-VIS (row 1) and Euclid J (row 2). 2nd column: 150 hours exposure. 3rd column: 150h hours exposure applying SR algorithm.*

5.8 Integration and test plan

5.8.1 Integration of the payloads

Four payload models will be developed: an initial **STM** to probe the concept and perform the first functional and environmental tests, an intermediate **EM** flight representative in form, fit and function of both flight payloads and will incorporate NIR detectors and ASICS with identical functionality as the science-grade units, a **QM** to qualify the design, and the final **FM**. QM and FM instruments will count with full flight design and standards except for NIR detector and ASICS of the QM.

Prior to the assembly of both iSIM-170 payloads, all manufactured pieces will be submitted to **quality control and measurement process** using a **CMM** to verify that every part complies with the dimensions and mechanical tolerance ranges defined by design.

The cameras will be assembled inside **ISO5 cleanrooms** with industry-standard cleanliness control procedures and performing optical alignment measurements to ensure both optical channels remain within the instrument's nominal tolerances.

Both payloads will be attached to the honeycomb optical bench structure (see section 5.5.1) by means of both mechanical and thermal interface, and the rest of the elements will be assembled around the basic structure to ease the integration. Electronic components and software will be checked to ensure a correct fit and connection of all the components. Since temperature stabilization requirements are critical for both instruments to perform as expected, all the interfacing elements will be thermally isolated using thermal washers, interfacing materials and other space-qualified methods. Intermediate measurements and alignment checks will be incorporated during the whole assembly process to meet the defined alignment specifications.

5.8.2 Validation and test plan

All the camera models will undergo the following test plan:

1. **Optical characterization in air and vacuum:** To prove the optical performance of the payload, PSF acquisitions will be done in two different setups: first in ambient conditions inside the ISO5 cleanroom, and then in vacuum in the TVC.
2. **Mechanical test:** The camera will be submitted to vibration tests to prove that it can withstand the launch environment without damage. Sine and random testing will be performed. Also, micro-vibration environment could be tested to ensure that the optical system is not affected by the disturbance created by adjacent elements.
3. **Thermal testing:** Also, thermal vacuum testing will be performed by simulating real mission conditions and probing the correct functioning of the TCS, which is critical for the thermal stabilization of the payload and its optical performance.
4. **Electronics testing:** All the electronic interfaces and the control PCB will be tested to ensure correct readings and functioning.

No shock or acoustic tests are foreseen for this stage.

After performing all the tests described above, the camera will be integrated inside the satellite platform and submitted to **system level test campaign**. These tests will include electrical unit tests (OBC, radios, antennas, power, sensors, actuators, and interface electronics), mechanical unit tests (structure and actuators), payload and satellite bus checkouts, communication tests and spacecraft functional, qualification and acceptance testing.

Besides the verification by test and inspection after every critical stage to ensure that no damage has occurred to any of the subsystems, previous design and analysis stages will be used as verification methods. During these phases, specialized software tools, including CAD, FEM, orbit simulation, thermal performance

(similar to the thermal analysis presented in section 5.5) and optical response will be used to drive the detailed design and deep analysis of both the payload and the influence of the rest of the elements inside the satellite.

5.9 Calibration plan

Flat-fields: The calibration plan of ARRAKIHS will be based on that of other similar larger observatories, with comprises a series of pre-launch and in-orbit calibration procedures. Pre-launch bias, darks and flats will serve as a prior for a series of time-monitored calibration frames. Flat fields will be obtained using a calibration ladder strategy as defined in Borlaff et al. 2022, 1) Ground-based flat priors, 2) Self-calibration flats using dithered observations of crowded star fields, and 3) Sky flat fields from calibration fields. While 1) and 2) are ideal for the calibration of pixel-to-pixel and very-large scale flat field spatial components, sky flats allow to monitor the appearance of bad pixels, or large-scale variations of the sensitivity due to ice-contamination, from pixel-to-pixel scales to the whole FOV. Combination of all these flat fields will be done following a delta-flat strategy. This technique has proven to be a valid method for correcting large-scale gradient residuals in the flat fields of the WFC3/IR and the ACS instruments of the Hubble Space Telescope (Pirzkal et al. 2011; Mack et al. 2018).

PSF: In-flight calibration of the PSF will be possible thanks to the use of calibration stars, following a procedure described in Trujillo et al. 2016. The combination of wide dithered observations of stars of different brightness will allow to generate PSF models as wide at twice the FOV of the detector (Infante-Sainz et al. 2020), a fundamental capability to correct the stray-light from in-field sources, and from the objects of interest themselves (Sandin et al. 2014, 2015).

6 PROPOSED MISSION CONFIGURATION AND PROFILE

In this section we describe the specific mission profile, orbit and spacecraft requirements, concepts of operations and existing launcher and platform solutions.

6.1 Mission profile

The ARRAKIHS mission will fly into a Low Earth Orbit (LEO) in a Sun-Synchronous Orbit (SSO) configuration, in an always illuminated orbit where it can keep the payload as thermally stable as possible and with maximum visibility of its targets. Keeping a low SSO allows for lower operational and launch costs. This SSO orbit is reachable from the Guiana Space Centre or even any major space port currently in service. The nominal duration of the scientific operations to observe all galaxy targets will be completed in a minimum time of 2 years, with the goal of extending the operation up to a total of 3 years. This orbit allows for ground station communications from 10 up to 17 minutes duration depending on the final selected height.

We derive the following requirements from the proposed mission and payload configuration:

- *Orbit & Launcher*
  - **Type**: LEO sun-synchronous orbit
  - **Height**: 600-1350 km
  - **Inclination**: 99.55º at 1000 km
  - **LTAN**: 6:00 AM or PM
  - **Total S/C mass**: < 350 Kg
  - **Total S/C volume**: 1550x1534x1154 mm
- *Spacecraft*
  - **Average P/L Power**: 120 W
  - **Peak P/L Power**: < 200 W
  - **P/L volume**: 590 x 471 x 610 mm^3
  - **Daily P/L transmission**: 5.5 GB
  - **S/C Storage capacity**: 3-day backup
  - **S/C Slew rate**: 1.5 deg / sec
  - **S/C Attitude and stability**
    - **Absolute Pointing Error** (APE): 20 arcsec
    - **Absolute Knowledge Error** (AKE): No requirement
    - **Relative Pointing Error** (RPE): 0.5 arcsec RMS
    - **Performance Drift Error** (PDE): < 50 mas

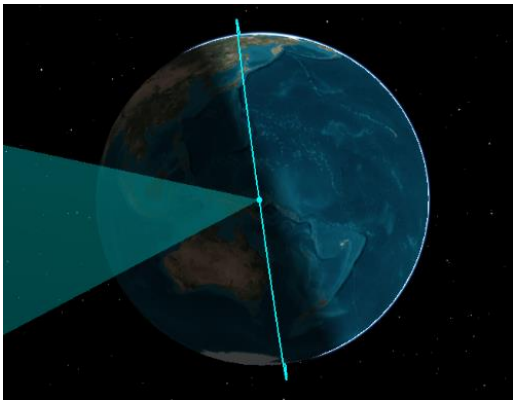

Figure 29: *ARRAKIHS SSO Orbit*

6.2 Concept of Operations (CONOPS)

Deriving from the scientific requirements, we identify the following observational constraints:

- Sun Aspect Angle: > 70 degrees
- Average Earth Surface Dip Angle: -24.14º @600 km / -30.32º @1000 km / -34.5º @ 1350 km
- 100 km Atmosphere Dip Angle: -22.05º @600 km / -28.76º @1000 km / -33.16º @ 1350 km
- Zodiacal light J-magnitude limit: 21.8 mag
- Galactic Plane Exclusion Angle: 20 degrees
- Dust Extinction Absorption limit E(B-V): < 0.105
- Stand-by ECS on South Atlantic Anomaly: 20 minutes for 6 to 8 orbits a day

With the following requirements we need to optimize the observability with minimal zodiacal light, maximum earth elevation, maximum Sun Aspect Angle and minimal slew offsets. We have analyzed two possible configurations as concept for operations:

- CONOPS- Mode A: The instrument observes towards the anti-sun direction, with a continuous visibility cone of +/- 20 degrees around the anti-sun, and an extended cone of +/-40 degrees, having to change target at least once for each orbit. The solar panels are always facing the sun and the optical system and radiators towards the anti-sun direction providing a thermally stable operation. This cone will drift by 0.98° a day from the background stars, allowing on the best cases to image targets for as long as 60 days continuously, or an average of 43 days.
    - Advantage: possibility to perform continuous observations and maximum sun separation.
    - Disadvantage: Observations around the ecliptic plane and with larger Earth's limb. No visibility around the ecliptic poles.

- CONOPS- Mode B: The instrument observes around the Earths Zenith at the 6 AM/PM SSO orbit, shifting between two targets per orbit. As in Mode A, the panels are facing the sun in a very stable thermal operation, with the instrument facing 90° from the anti-sun coordinate and towards the vertical orientation of the spacecraft. We maintain a +70° to +130° Sun Aspect Angle to allow flexibility to observe objects that are not exactly at the corresponding Right Ascension, while maintaining the sun away from the FoV and aligned with the panels. Throughout the year all objects are visible twice in this mode.
    - Advantage: All latitudes and longitudes visible. Larger separation from Earth's limb and ecliptic plane.
    - Disadvantage: No continuous visibility of targets resulting in higher number of slews.

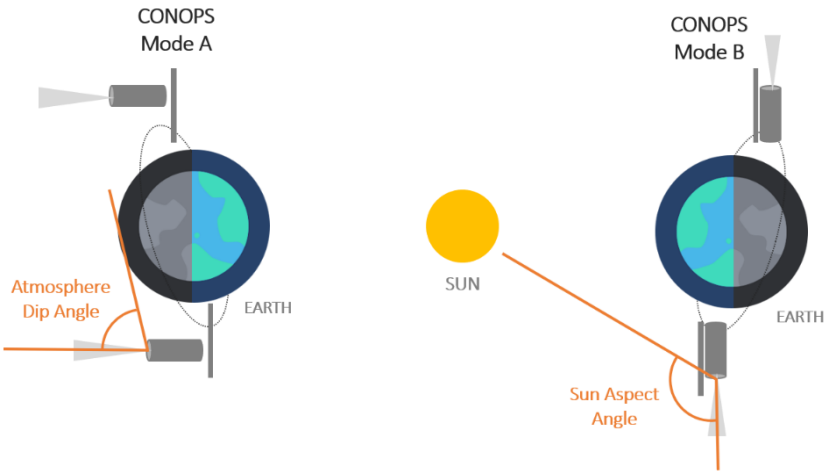

Figure 30: The two CONOPS modes identified for the mission

We performed a study to evaluate the visibility and background performance of both configurations. Mode A is more sensitive to orbit altitude as it does observe closer to the atmosphere. Mode B has on average 1 magnitude fainter background due to Zodiacal Light than Mode A. The mean elevation from earth (considering 100 km atmosphere) is approximately 12 degrees higher in Mode B. Both ascending nodes at 6 AM and 6 PM behave similarly to the current target selection. The configuration that delivers the best mission performance is CONOPS Mode B, at 1000 km altitude and ascending node at 6 PM. However, the differences in altitude and ascending node are minor and the other orbit profiles are also compliant with the scientific requirements, enabling flexibility for the launch service.

At 1000 km altitude, we will have approximately 14 orbits per day, 13 of which will devoted for science observations and 1 for calibration and downlink purposes.

Currently the effects of the SAA on the science observations have not been assessed, for this reason a worst-case scenario has been considered in which the science instruments will not take science or calibration data while crossing it. For this reason, a down time between 20 to 30 minutes for 6 to 8 orbits has been taken into account.

At heights above 1350km the S/C would not suffer eclipse periods, while at 600km the eclipse season would last for 3 months with a maximum of 20 minutes per orbit on the solstice. The S/C thermal system will be designed to minimize the downtime period during the eclipse season and the height of the orbit will be chosen to minimize the launch costs while minimizing the duration of the eclipse season.

6.2.1 Science observations orbit

The science observations will be made as set of 10-minute dither exposures. Each target will be observed 150 hours, combining 900 dither observations. At the beginning the spacecraft will have to slew to the desired target position (unless it is already in place from previous observations) and after preparing flushing the residual charges, the FGS system starts, and the exposure starts and integrates for 10 minutes. Then the electronics begin the detector readout and the satellite dithers slightly as a result of the disabled FGS, without any commanded movement in about 10 seconds (more time can be allocated if necessary). The instrument will keep performing observations until the target is expected to be out of visibility or the observations for the target are completed. Then the spacecraft slews to a new visible target.

6.2.2 Calibration & downlink observations orbit

One orbit is expected to be dedicated for calibration and downlink purposes a day. A set of darks (zero exposure) and flats will be observed, in addition to other calibration fields such as open clusters or spectrophotometric standard stars. Additionally, the satellite will reorient its antenna to perform the downlink transmission when passing over the corresponding ground station.

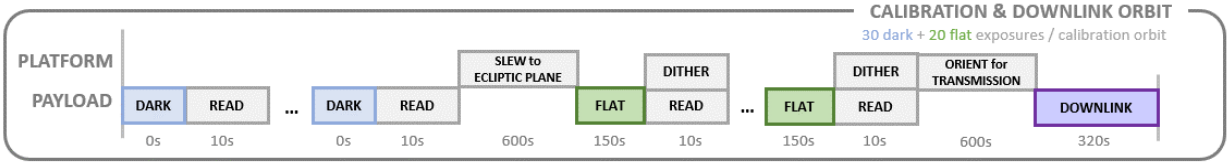

6.3 Launcher

Currently the payload mass is expected to be < 60 kg and the spacecraft dry mass is estimated to be < 300 kg. Therefore, the estimated mass of the spacecraft is well below the limits of the launch mass for the Vega-C launcher at the highest proposed orbit and could be part of a Small Spacecraft Mission Service to minimize costs, as long as the S/C is launched at SSO on the correct LTAN orbit. Launch of the ARRAKIHS satellite is today targeted not earlier than 2029.

Example of SSMS FLEXI-4 configuration.
ARRAKIHS position in blue.

Example of VESPA configuration.
ARRAKIHS spacecraft could fly below or above the VESPA+R structure.

Launch Vehicle Configurations considering spacecraft's mass and volume defined above, the contemplated launch configurations could be:

- A dedicated launch with the ARRAKIHS satellite
- In a double or shared launch configuration with third party customer(s), ARRAKIHS being the main customer if the orbit parameters are compatible with the mission.
- In a Small Spacecraft Mission Service if the orbit parameters are compatible with the mission.

Arianespace proposes to launch the ARRAKIHS satellite either in a dedicated launch onboard a VEGA-C Launch Vehicle or on a VESPA double launch structure allowing to embark: A main passenger on top of the VESPA structure and one or several micro or nanosatellites under the VESPA. The current proposed platforms would allow to fly inside the VESPA structure or on top of it.

6.4 Spacecraft

6.4.1 Existing platforms & required modifications

Below we identify solutions that meet the specified ARRAKIHS spacecraft requirements on already existing solutions, each of the proposed platforms come with a fine AOCS however because the attitude requirements for this mission are very strict, the option of using a "High-Performance AOCS" on top of their platform for science observation has been studied and proposed below the proposed platforms. The currently proposed platforms have already been designed or flown and they would require minimal modifications and thus rely on a high TRL initial status:

6.4.1.1 AIRBUS Solution

The proposed satellite design is composed by a prismatic body platform, where the instrument is mounted on its top surface, plus three body-mounted solar array panels. There is a fixed sunshield in the central solar panel, to provide the required shadow to Instrument radiators. The structure design is made of sandwiches with metallic skins for top-bottom-side panels. The panels accommodate the platform and instrument equipment. The top surface of the platform prismatic structure is dedicated to the accommodation of the Instrument elements. The bottom panel holds the propulsion subsystem, launcher interface, and other units such as the reaction wheels. The 4 wheels are mounted on dedicated brackets, including micro-vibration dampers. Their thermal control is based on radiative exchange. Specific brackets to be attached to the external surfaces will be designed to support any sensor, instrument or antenna, etc. The star trackers optical heads and the gyroscope will be accommodated in the payload to minimize

thermoelastic deformation. The wet mass budget of the spacecraft is 300 kg considering an instrument mass of 50 kg and a platform of 220 kg, plus the 30 kg for the propellant.

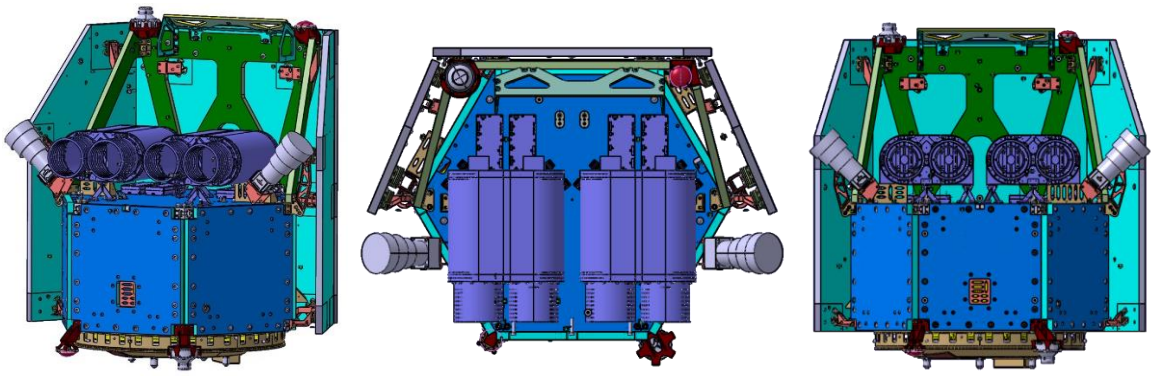

Figure 31: *The platform solution from AIRBUS for the ARRAKIHS Mission*

A thermal solution including passive cooling with MLI, radiator foils, black coatings and active thermal control to maintain the desired optomechanical and detector target temperature is also proposed. The electrical architecture and power subsystem allows to reach the required power by the payload, with solar array preliminary sizing for worst case (EOL) results in an area of 1.1 m2 for each lateral solar panel, and 1.5 m2 for the central panel. The design considers two extreme situations (assuming an extended angle with respect to the perpendicular to the orbit plane of ±60°):

- Observation during equinoxes. Angle with respect to anti-Sun direction in range -50.5° (one half of the orbit) to +69.5° (the other half).
- Observation on each solstice. Angle with respect to anti-Sun direction between these two values: -93° to +27.5° (or opposite signs).

An AOCS and Propulsion system based on existing platforms is proposed.

- Multi-head stellar trackers in hot redundancy
- Medium performance gyroscope
- A cluster of four reaction wheels
- Three internally redounded magnetorquers (for wheels offloading)
- Monopropellant propulsion (1N thrusters)

In combination of the payload FGS at 1Hz and centroid accuracy better than 0.12 arcsec, the RPE of 0.5” RMS is achieved.
The communication system would use X band for science data download plus a standard S-Band solution for TMTC communication.

6.4.1.2 OHB Solution

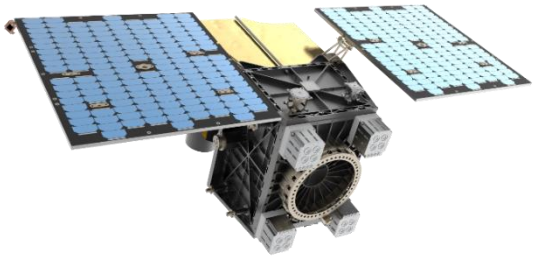

The **Innosat platform** is well suited to meet all the main ARRAKIHS platform requirements:

- ✓ Sun Synchronous observations at LEO 600-1000 Km
- ✓ ARRAKIHS payload module
- ✓ a pointing stability of 0.5 arcsec RMS over 10-minute nominal exposure
- ✓ radiators for passive cooling of 4x detectors at 140-150K

Main modifications:

- Payload accommodation, including concept for passive cooling
- Implementation of single point failure tolerance expected to be required

Satellite dimension and mass

- Satellite dimensions with payload volume in line with ARRAKIHS requirement (590*471*610 mm)
- Power system sizing needed to decide solar array size depending on final orbit choice and CONOPS
- Satellite mass estimate:
    - Payload 40-60 kg
    - Platform 120-140 kg (depending on power sizing, SPF requirement, equipment selection)
    - Margin 20%
- Total mass ~250 kg

Control of detector temperatures with passive radiator coolers

The following solution could be proposed based on heritage from earlier ESA missions.

1) The coupling of detectors to cooler can be done as on XMM/EPIC
2) The general use of three-stage passive coolers as used on XMM and METOP
3) Ensure to have sun-shields and Earth IR shields throughout the orbit including for all slewing directions. The implementation of such shields for your particular mission needs to be properly studied during the Phase A, but such shields should not in themselves be very difficult to implement.

Pointing accuracy

All bias errors disappear when optical payload is used as primary attitude sensor. All slew errors related to frame transformation also disappear. RW torque disturbances are reduced by using a smaller wheel. This reduces the slew rate to 20 deg/min which is deemed sufficient for ARRAKIHS with at most one slew per orbit. InnoSats high performance fiber optic gyro is operated at 10Hz with 1Hz measurement updates from the *Payload in the loop*. The following performance from the payload FGS is assumed: a FoV spatial error: 0.1" (3σ), Pixel spatial error: 0.1" (3σ), Temporal noise: 1" (3σ), About boresight performance is assumed to be x7 worse than across boresight performance. Compliance to the 0.5" RMS APE requirement is achieved with the above assumptions, InnoSats smallest wheel choice, and InnoSats high performance fiber optic gyro.

6.4.2 High-Performance AOCS

The Euclid mission had a strict pointing requirement of 75 milli-arcsec during the 565 sec exposure time, necessary to ensure a good quality PSF that required for the weak lensing measurements. Here we take advantage of the heritage from this high-performance AOCS and SENER proposes an equivalent solution that meets ARRAKIHS AOCS requirements.

Downsizing from Euclid spacecraft, we estimate an inertia of 230 kgm^2 around x- and y-axis and 180 kgm^2 around z-axis, for ARRAKIHS (dimensions are 1.64 x 1.64 x 2.08 m). The following disturbances are estimated at 700 km altitude:

- Solar Radiation Pressure torque: 0.022 mNm
- Gravity Gradient torque: 0.08 mNm
- Atmospheric drag torque: 0.52 µNm (negligible)

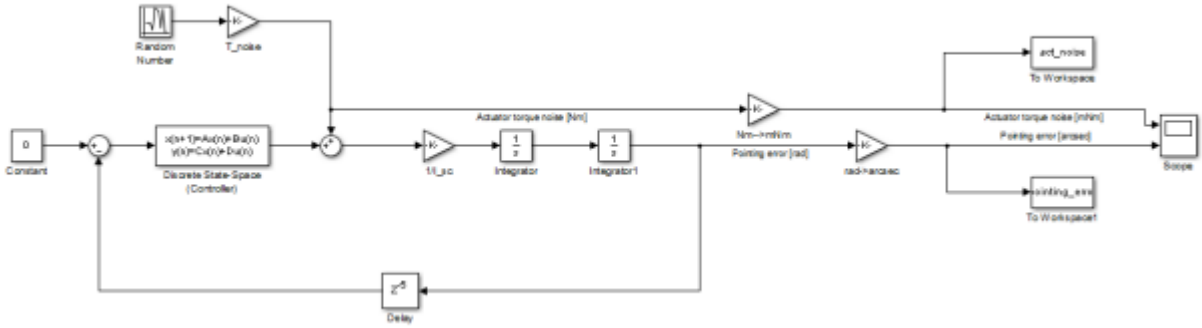

The following scenarios were studied:

- **Science mode:** Reaction wheels (RWLs) vs Micro Propulsion Subsystem (MPS)
- **Large Slews**: Reaction wheels (RWLs) vs Reaction Control Subsystem (RCS)
- **Transitions between large slews and science mode:** RCS vs RWL
- **Navigation:** FGS + Kalman Filter + Gyro

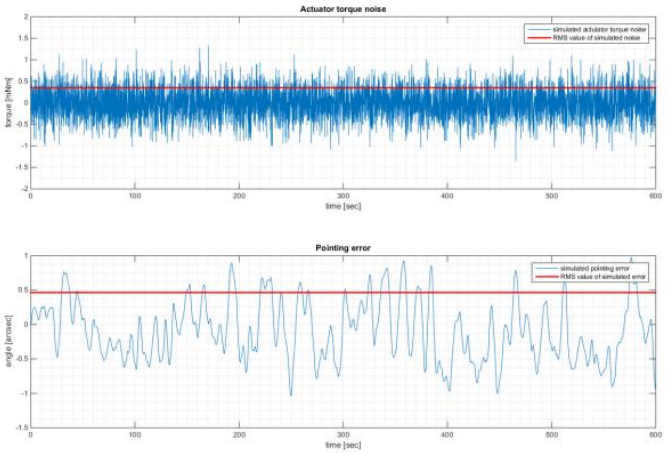

***Figure 33**: AOCS simulation study from SENER*

Performing the ARRAKIHS scientific observations using small RWLs is very challenging. Commercial RWLs are available for meeting the torque requirements, but the issues related to the storable momentum and LEO external perturbations might discard them as a valid option. Micro Propulsion Subsystem (MPS) can be used instead for the fine pointing (as it has been developed for Euclid's mission), requiring a reasonable amount of propellant for the entire mission (coarse preliminary estimation of 30 kg). Of the identified potential AOCS actuator configurations, two are identified as promising candidates:

1. **MPS** for science observations and **RCS** for large slews.
    a. It is the least complex of the two options and eliminates all RWL-related issues such as micro-vibrations, torque noise perturbations, momentum unloading, etc.
    b. The required RCS propellant seems reasonable provided that the average slew rotation is less than 180 degrees, which is used in this analysis as reference.
    c. The RCS thruster MIB will lead to a residual angular momentum during the transition between large slews and science observation → this needs to be compensated by MPS after entry in science mode → further analysis is required to quantify its impact.
2. **MPS** for science observations and **RWL** for large slews.
    a. This solution is more complex as it requires an additional actuator type (note that RCS is assumed to be present for safe mode) but requires less total mass as no RCS fuel is consumed during slews.
    b. The RWLs need to be stopped during science observation in order not to affect the pointing performance, which requires a dedicated process.
    c. Accumulation of angular momentum during large slews needs to be unloaded at the entry of science mode → a feedforward compensation of the external torques (SRP, gravity gradient, and drag) by MPS during the slews is highly recommended, which would significantly reduce the residual angular momentum at the entry of the science observation phase.

More analyses at more mature stages of the project are required to properly trade-off the propellant consumption and the transition times from slew to science. Of special relevance is the residual angular momentum at the end of the slew prior to entering the science phase as it will affect the time needed for the MPS to perform the momentum reduction and resulting pointing corrections. This may in fact tip the balance to either of the two configurations. It is also of relevance to note that the MPS has limited torque authority to perform relatively large rotations during the dithers. Consequently, it is recommended to maintain the dither rotations as small as possible at mission design level. A system requirement is recommended at spacecraft design level to minimize the systematic external perturbation torques, i.e., allocating the center of pressure (for drag and solar radiation pressure) near the center of mass, and/or avoiding mass distributions leading to high gravity gradient torques. Naturally, the project is required to be in a more mature stage for these analyses to be carried out. Future and better-defined requirements may change the design.

7 MANAGEMENT SCHEME

7.1 Project management

ARRAKIHS is a "Fast" mission to be led by ESA, proposed by the ARRAKIHS Mission Consortium (AMC), a group of 8 entities representing 7 countries (i.e., Austria, Belgium, Spain, Sweden, Switzerland, United Kingdom, United States), coordinated by the Spanish IFCA. A dedicated **Project Manager** will be appointed to ensure an effective coordination among the different parties of the Consortium and with ESA to keep track of the project implementation and to perform day-to-day tasks related to the activity.

The following image presents a high-level distribution of roles between ESA and the AMC. The AMC will perform tasks and activities as agreed with and in support of ESA, leader of the Mission. The **top level** of the diagram includes the Project Office activity, to be performed by both ESA and the AMC separately but also in coordination, as evidenced by the double line connecting the blocks. Each party will have a separate activity related to science, i.e., Project Scientist on ESA side and Core Team for AMC. The **second level** refers to the main activities of the project, i.e., Instrument and Science on AMC side, and Launch, Spacecraft and Ground segment on ESA side. The blocks Ground segment and Instrument foresees a participation of both parties for specific tasks, as specified in the sections below, and thus are connected with dashed lines.

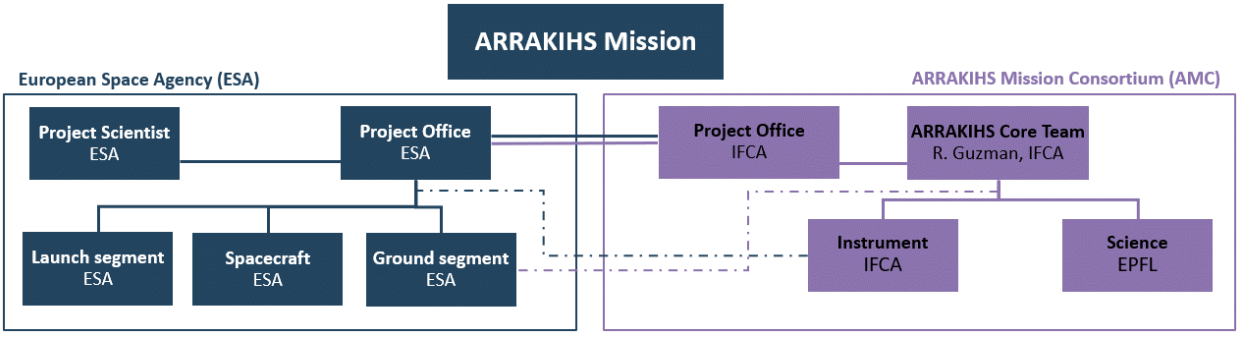

7.1.1 Share of responsibilities & Procurement scheme

As explained above, a clear boundary of responsibilities between ESA and the AMC has been defined, and the alignment between the two sides will be guaranteed by the project management and the project office. The distribution of responsibilities will consist of the following.

ESA will oversee and procure, through the F-mission funding:

- **Launch segment**, including the launch opportunity and related services.
- **Space segment** will be shared, and it is proposed that the Agency will be in charge of

- the satellite platform to board the instrument developed by AMC.
- a component of the instrument itself, i.e., detectors and front-end electronics.

- Ground segment will be shared, with the Agency being in charge of:
  - the Ground Stations, support telemetry and communications with the spacecraft.
  - the Mission Operations Centre (MOC), operation of ground stations and spacecraft orbit, tele-commanding, monitoring and telemetry reception.
  - the Science Operations Centre (SOC), scientific mission planning, instrument operations, quick look analysis, data archival.

AMC will oversee and procure, by means of European and National funding programs:

- Space segment, for which AMC will be responsible for the payload development and delivery.
- Ground segment, with AMC responsible for
  - the Science Data Center (SDC), data processing and instrument specific algorithms. Scientific analysis and simulations.
  - the SOC mirror, as interface with the elements provided by ESA.

This distribution is shown in the following schema:

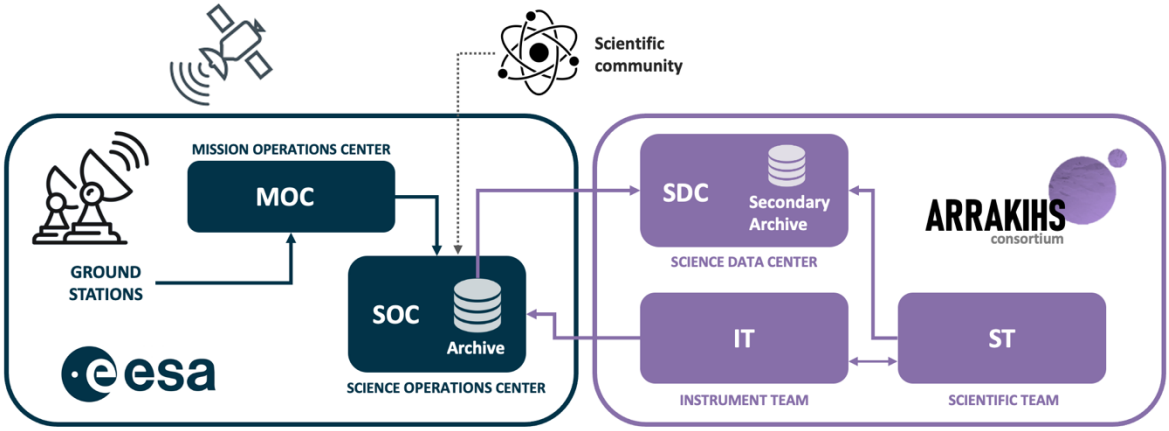

7.1.2 National agencies

The AMC will be supported by the National agencies of their respective countries, that agreed to contribute to the procurement for the ARRAKIHS Mission. These agencies include Austrian Research Promotion Agency (FFG), Belgian Science Policy Office (BELSPO), Centro para el Desarrollo Tecnológico Industrial (CDTi), Agencia Estatal para la Investigación (AEI), Swedish National Space Board (SNSB), Swiss Space Office (SSO) and United Kingdom Space Agency (UKSA). All agencies have confirmed their support for this project and committed to make it official in a letter sent to ESA by September 15, 2022.

7.1.3 ARRAKIHS Consortium organisation

The management structure of the mission we are proposing foresees an ESA-led organization, sharing responsibilities with the AMC. The AMC will be led by the Principal Investigator of this proposal, Dr. Rafael Guzman, professor at both IFCA-CSIC and UF. The AMC will be composed by three main groups:

(1) The ARRAKIHS Scientific Team (AST) will be led by the Scientific Coordinator, Prof. Pascale Jablonka. It is composed of the core team described above, plus the following additional researchers that communicated their interest and commitment to participate to the mission:

Science Team	Center
Joao Alves	University of Vienna
Rita Belén Barreiro Vilas	IFCA
Alberto Fernandez Soto	IFCA
Alejandro Camazon	University of Florida
Francisco Javier Casas	IFCA
Francisco Javier Castander Serentill	ICE
Andrew Cooper	National Tsing Hua Univ
Diego Herranz	IFCA
Jesús Gallego Maestro	UCM
Artemio Herrero	University of La Laguna
Pascale Jablonka	EPFL
Bradley J. Kavanagh	IFCA
Antonio Marín Franch	CEFCA
Enrique Martínez González	IFCA
Miguel Mas	CAB-CS/INTA
Lucio Mayer	University of Zurich
Göran Ostlin	Uppsala University
Yves Revaz	EPFL
Santi Roca-Fabregas	UCM
Isabel Santos-Santos	ICC/University of Durham
Alejandro S. Borlaff	NASA Ames
Patricio Vielva	IFCA

Core Team	Center
Rafael Guzmán	IFCA
Oscar Agertz	University of Lund
Michaël De Becker	University of Liège
José María Diego	IFCA
Denis Erkal	University of Surrey
Mariángeles Gómez-Flechoso	UCM
Manuel Güdel	University of Vienna
David Martínez-Delgado	IAA
Ben Moore	University of Zurich
Santiago Serrano	ICE/Satlantis
Paul Torrey	University of Florida

These institutions will provide the necessary researchers to support the scientific tasks assigned in the various phases of the mission. The AST will be in charge of defining the scientific requirements that will flow down to the rest of the components for the success of the mission.

(2) The Instrument Team will be coordinated by the PI, Prof. Rafael Guzmán. This group will be required to communicate with ESA and with the platform provider during its development phases and with SOC for calibration purposes during the operation phase.

(3) The Science Data Center will be set to support the ground image processing, planned to be hosted by IFCA, which holds the Altamira HPC cluster with extensive processing and archive capabilities. The SDC will be coordinated by the SDC lead, Dr. Jose Maria Diego from IFCA. In coordination with the SOC, the SDC will implement and orchestrate the instrument specific algorithms as well as the production of accurate simulations that will provide key information to evaluate the scientific mission performance.

7.1.4 Science Management

The AST will be in charge of the activities related to science management, throughout the entire mission, such as:

- Scientific requirements
- Support mission performance evaluations
- Survey strategy and calibration plan
- Data analysis and quality assessment
- Definition of publication rules
- Scientific exploitation
- Public outreach and communication

All the activities will be held within and by the AST, in coordination with ESA Project Scientists, to define the approach and procedures to maximise the scientific outcome, for the benefit of both the AMC and the

broader scientific community, according to ESA guidance. The AST will review the Instrument and Science tasks at each stage from a scientific perspective to ensure compliance with the primary scientific goals.

7.1.5 Data policy & Community involvement

The ARRAKIHS consortium is aware of the novelty of the mission data and the large interest of the scientific community in high-quality data of low surface brightness imaging of the Universe. Additionally, the versatility of the data will allow to tackle a large number of ancillary scientific cases, as it is detailed in the science section. For this reason, a quick access of the scientific community to reliable data is desirable. For these motivations, together with the consortium policy of contributing to the scientific progress, a special effort will be made to share the mission data and results with the scientific community as soon as possible.

The analysis and processing of the data will be led by the ARRAKIHS consortium scientists. The main goal is to obtain science-quality data as soon as possible providing free access to the scientific community at large. The schedule for the data sharing is designed to guarantee a correct calibration and image processing using a pipeline developed by the ARRAKIHS consortium, as follows:

1) Between twelve and eighteen months after launch, the fully reduced images of three galaxy halos will be published (Data Release 1, or DR1). This first data release will demonstrate the scientific potential of the ARRAKIHS mission.
2) At the end of two years after the launch, a new set of images consisting of fully calibrated and processed images of thirty galaxy halos will be published (DR2).
3) The final publication of the entire dataset, including all the observed halos fully calibrated and processed, with the multi-wavelength information, will take placed approximately two years after the end of the mission (DR3).

Access to the three data releases will be open to the entire scientific community and collaborations for the data publication will follow general standards in data archiving.

7.2 Implementation plan and project schedule

As mentioned above, the mission foresees a clear distribution of responsibilities and tasks between ESA and the AMC, as can be seen in the following diagram:

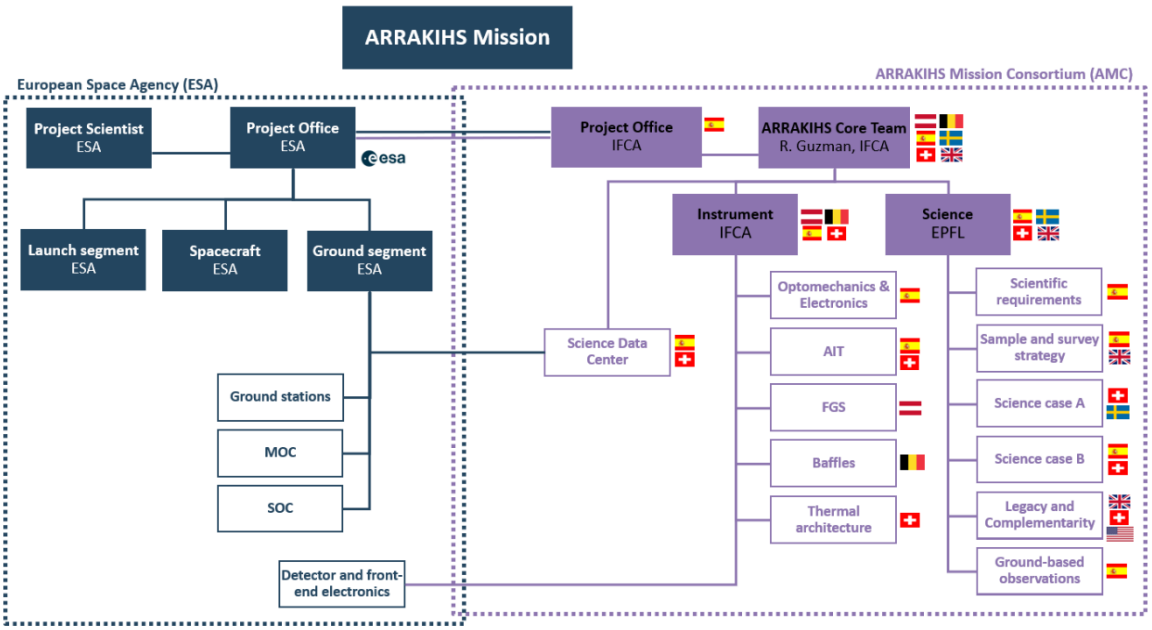

The left part of the diagram includes the tasks to be performed by ESA, while the right part shows the activities to be performed by the Consortium. Although a clear separation is visible, it is important to note that a strong coordination and communication is foreseen for the Project Office task, where the AMC project manager will support the overall leadership of ESA for the mission.
The top-level activity blocks specify the leader of the activity, which will be in charge of overseeing and coordinating the lower-level tasks. The national flags of the involved entities indicate the participation of different partners per each activity and are reported in the top-level block to represent the collaborative framework that the AMC will apply throughout the implementation.
The AMC portion of the project will be managed by IFCA, that will also act as interface with ESA, to maintain the Agency up to date, assure a smooth implementation and harmonize the activities split among the different actors. To guarantee an effective coordination, a dedicated project manager will be appointed by IFCA and AMC, with the necessary experience and expertise to perform the duties at hand.

A high-level description of the top-level activities of the Consortium is presented below.

Activity:	Science		
Leader:	P. Jablonka	**Contributor(s)**:	IFCA, UCM, IAA, ICE, CAB, UZH, Lundt, U. Surrey, U. Durham, U. Vienna, U. Liège, UF
Main objectives: This activity is the starting point of the mission and regards the collection of inputs by the AST based on relevant study cases and state-of-the-art. The team will define a strategy for sampling and surveying and take into account previous and/or ongoing endeavours in the field and any complementarity aspect that could benefit the mission. Other inputs will be collected from ground-based observations, in a holistic approach. The main goals will be to assess the scientific added-value and feasibility of the proposed methods, and to derive requirements to be used for the mission implementation, the instrument development, and the operations at ground segment level.			

Activity:	Instrument		
Leader:	R. Guzmán	**Contributor(s)**:	IFCA, ICE, CAB, MSSL, U. Vienna, Satlantis, APCO, CSL, UF
Main objectives: This activity focuses on the development of the mission's Instrument, starting from the scientific and technical requirements, and following all phases of study up to a consolidated design (0/A/B), then entering the fabrication and testing phases (C/D), before the flight readiness and launch of the instrument. The activity includes the development of every component of the instrument, including the element proposed to be procured by ESA (detector and front-end electronics). Different partners of the Consortium will contribute to the development, all coordinated and harmonised by IFCA.			

Activity:	Ground Segment - Science Data Center		
Leader:	J.M. Diego	**Contributor(s)**:	IFCA, IAA, ICE, UZH
Main objectives: This activity will use the previous tasks results as inputs to define the Science Data Center architecture and best approach for data analysis and processing, in connection with the selected observations strategy and within the overall frame of the ground segment managed by ESA, that will also oversee the ground stations network, MOC and SOC. The Science Data Center will include an archive to store and catalogue data, and to allow access to products.			

An alternative representation of the work to be performed can be found in the following graph, where the different phases, expected timeframes and milestones are displayed (*note: the chart has been divided in two lines for visibility purposes only*).

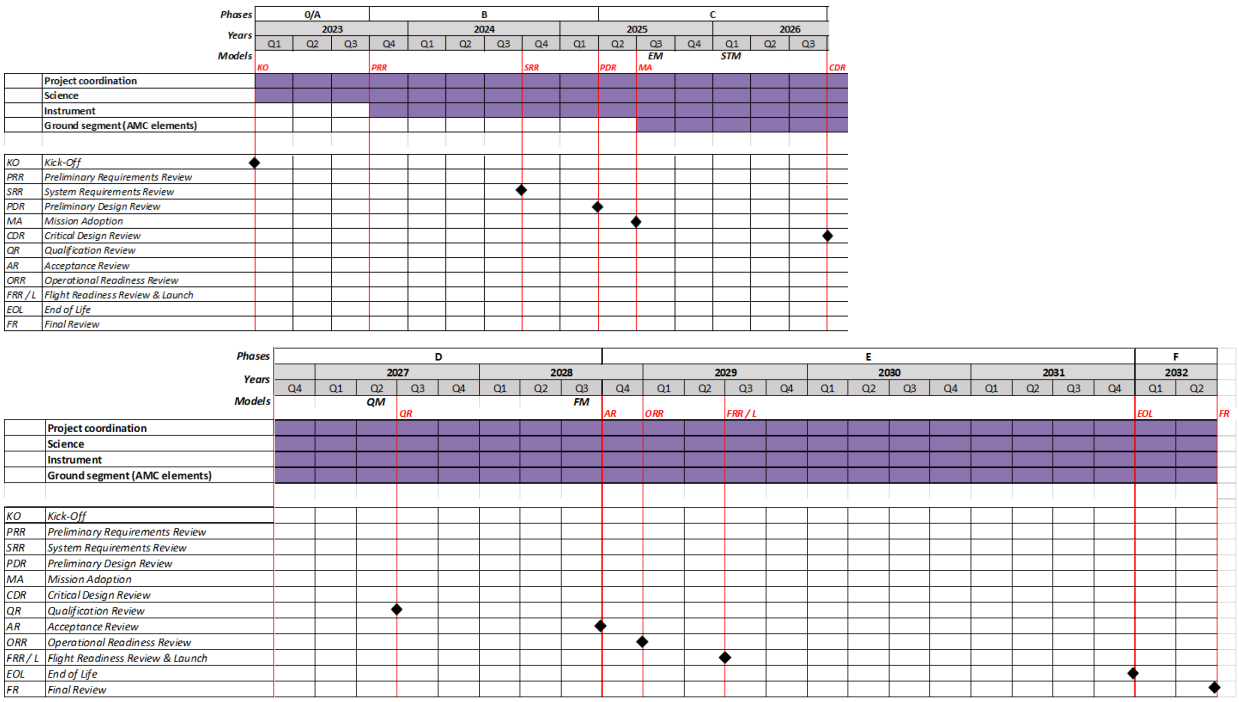

The duration of each **phase** has been assigned based on ESA requirements and the Call for Proposal indicative timeframe.
Besides the **milestones** represented by meetings and reviews to be held between the Consortium and the Agency (i.e., KO, PRR, SRR, PDR, MA, CDR, QR, AR, ORR, FRR, EOL, FR), the graph above also indicates the expected readiness of the instrument **models** (i.e., EM, STM, QM, FM).
The Reviews listed above will be organised by the project manager appointed by the Consortium, who will notify and invite ESA representatives to each meeting, share an agenda, coordinate the meeting execution, share minutes and relevant material afterwards, update the list of actions to be implemented. Any deviations of the expected schedule, tasks, or milestones, will be promptly communicated to ESA, and contingency measures will be adopted where necessary.
A summary of each phase milestones can be found in the following table:

Phase	Duration	Milestones	Models
0/A	Q1 2023 – Q3 2023	KO, PRR	--
B	Q4 2023 – Q1 2025	SRR, PDR	--
C	Q2 2025 – Q3 2026	MA, CDR	EM, STM
D	Q4 2026 – Q3 2028	QR, AR	QM, FM
E	Q4 2028 – Q4 2031	ORR, FRR / L, EOL	--
F	Q1 2032 – Q2 2032	FR	--

The milestones, models and reviews have been assigned to each phase according to standard practices and ECSS guidelines. A specific milestone called MA (Mission Adoption) has been included as per the Call for Proposals documentation.
Besides these formal steps, regular **progress meetings** with ESA will be organized within the shared project office activity, to report on completed tasks, ongoing activities, and next steps of the implementation.

8 BIBLIOGRAPHY

[1]Bahcall, N. A., Ostriker, J. P., Perlmutter, S., and Steinhardt, P. J., “The Cosmic Triangle: Revealing the State of the Universe”, Science, vol. 284, p. 1481, 1999. doi:10.1126/science.284.5419.1481.

[2] Klypin, A., Kravtsov, A. V., Valenzuela, O., & Prada, F. “Where Are the Missing Galactic Satellites?” The Astrophysical Journal, vol. 522 p.82–92, 1999. doi: 10.1086/307643.

[3] Ferreira, E. G. M., “Ultra-light dark matter”, Astronomy and Astrophysics Review, vol. 29, no. 1, 2021. doi:10.1007/s00159-021-00135-6.

[4]Santos-Santos, I. M., Domínguez-Tenreiro, R., and Pawlowski, M. S., “An updated detailed characterization of planes of satellites in the MW and M31”, Monthly Notices of the Royal Astronomical Society, vol. 499, no. 3, pp. 3755–3774, 2020. doi:10.1093/mnras/staa3130.

[5] Pawlowski, M. S. The planes of satellite galaxies problem, suggested solutions, and open questions. Modern Physics Letters A, 33(6):1830004, 2018. doi: 10.1142/S0217732318300045.

[6] Kashlinsky, A., Arendt, R. G., Mather, J., and Moseley, S. H., “Tracing the first stars with fluctuations of the cosmic infrared background”, Nature, vol. 438, no. 7064, pp. 45–50, 2005. doi:10.1038/nature04143.

[7] Martínez-Delgado, D., “Tracing satellite planes in the Sculptor group. I. Discovery of three faint dwarf galaxies around NGC 253”, Astronomy and Astrophysics, vol. 652, 2021. doi:10.1051/0004-6361/202141242.

[8] Pedani, M., “Sky surface brightness at Mount Graham II. First JHKs science observations with the Large Binocular Telescope”, New Astronomy, vol. 28, pp. 63–69, 2014. doi:10.1016/j.newast.2013.10.005.

[9] Moore, B., “Dark Matter Substructure within Galactic Halos”, The Astrophysical Journal, vol. 524, no. 1, pp. L19–L22, 1999. doi:10.1086/312287.

[10] Carlin, J. L., “Tidal Destruction in a Low-mass Galaxy Environment: The Discovery of Tidal Tails around DDO 44”, The Astrophysical Journal, vol. 886, no. 2, 2019. doi:10.3847/1538-4357/ab4c32.

[11]Wetzel, A. R., Hopkins, P. F., Kim, J.-. hoon ., Faucher-Giguère, C.-A., Kereš, D., and Quataert, E., “Reconciling Dwarf Galaxies with ΛCDM Cosmology: Simulating a Realistic Population of Satellites around a Milky Way-mass Galaxy”, The Astrophysical Journal, vol. 827, no. 2, 2016. doi:10.3847/2041-8205/827/2/L23.

[12] Sales, L. V., Wang, W., White, S. D. M., and Navarro, J. F., “Satellites and haloes of dwarf galaxies”, Monthly Notices of the Royal Astronomical Society, vol. 428, no. 1, pp. 573–578, 2013. doi:10.1093/mnras/sts054.

[13] Wheeler, C., “Sweating the small stuff: simulating dwarf galaxies, ultra-faint dwarf galaxies, and their own tiny satellites”, Monthly Notices of the Royal Astronomical Society, vol. 453, no. 2, pp. 1305–1316, 2015. doi:10.1093/mnras/stv1691.

[14] Santos-Santos, I. M. E., Fattahi, A., Sales, L. V., and Navarro, J. F., “Magellanic satellites in ΛCDM cosmological hydrodynamical simulations of the Local Group”, Monthly Notices of the Royal Astronomical Society, vol. 504, no. 3, pp. 4551–4567, 2021. doi:10.1093/mnras/stab1020.

[15]Boylan-Kolchin, M., Bullock, J. S., and Kaplinghat, M., “Too big to fail? The puzzling darkness of massive Milky Way subhaloes”, Monthly Notices of the Royal Astronomical Society, vol. 415, no. 1, pp. L40–L44, 2011. doi:10.1111/j.1745-3933.2011.01074.x.

[16] Boylan-Kolchin, M., Bullock, J. S., and Kaplinghat, M., “The Milky Way's bright satellites as an apparent failure of ΛCDM”, Monthly Notices of the Royal Astronomical Society, vol. 422, no. 2, pp. 1203–1218, 2012. doi:10.1111/j.1365-2966.2012.20695.x.

[17] Tulin, S. and Yu, H.-B., “Dark matter self-interactions and small scale structure”, Physics Reports, vol. 730, pp. 1–57, 2018. doi:10.1016/j.physrep.2017.11.004.

[18] Javanmardi, B., “DGSAT: Dwarf Galaxy Survey with Amateur Telescopes. I. Discovery of low surface brightness systems around nearby spiral galaxies”, Astronomy and Astrophysics, vol. 588, 2016. doi:10.1051/0004-6361/201527745.

[19] Henkel, C., Javanmardi, B., Martínez-Delgado, D., Kroupa, P., and Teuwen, K., “DGSAT: Dwarf Galaxy Survey with Amateur Telescopes. II. A

catalogue of isolated nearby edge-on disk galaxies and the discovery of new low surface brightness systems", Astronomy and Astrophysics, vol. 603, 2017. doi:10.1051/0004-6361/201730539.

[20] McConnachie, A. W., "The Observed Properties of Dwarf Galaxies in and around the Local Group", The Astronomical Journal, vol. 144, no. 1, 2012. doi:10.1088/0004-6256/144/1/4.

[21] Mao, Y.-Y., "The SAGA Survey. II. Building a Statistical Sample of Satellite Systems around Milky Way-like Galaxies", The Astrophysical Journal, vol. 907, no. 2, 2021. doi:10.3847/1538-4357/abce58.

[22] Martin, N. F., "The PAndAS View of the Andromeda Satellite System. II. Detailed Properties of 23 M31 Dwarf Spheroidal Galaxies", The Astrophysical Journal, vol. 833, no. 2, 2016. doi:10.3847/1538-4357/833/2/167.

[23] Hosek, M. W., "SPISEA: A Python-based Simple Stellar Population Synthesis Code for Star Clusters", The Astronomical Journal, vol. 160, no. 3, 2020. doi:10.3847/1538-3881/aba533.

[24]Fouesneau 2022; https://urldefense.proofpoint.com/v2/url?u=https-3A__github.com_mfouesneau_pyphot&d=DwIDaQ&c=sJ6xIWYx-zLMB3EPkvcnVg&r=_t6FjN5_WXdeCB1WqutqxDYKtHVsetBZ2ZLZzYWKn4s&m=pmV0nrMBS5qWAytN62CUTsoZQHlJ9-4GXkTxCjKEhK5tVPW3_77L3sBVNyA41Mhe&s=qEnrFOczvNAtdnl-bT_5jXmztDm9pWb1c1JQCWQYCmg&e=

[25] Courteau, S., "Galaxy masses", Reviews of Modern Physics, vol. 86, no. 1, pp. 47–119, 2014. doi:10.1103/RevModPhys.86.47.

[26] Crnojević, D., "The Faint End of the Centaurus A Satellite Luminosity Function", The Astrophysical Journal, vol. 872, no. 1, 2019. doi:10.3847/1538-4357/aafbe7.

[27] Helmi, A., "Streams, Substructures, and the Early History of the Milky Way", Annual Review of Astronomy and Astrophysics, vol. 58, pp. 205–256, 2020. doi:10.1146/annurev-astro-032620-021917.

[28] Martínez-Delgado, D., "Stellar Tidal Streams in Spiral Galaxies of the Local Volume: A Pilot Survey with Modest Aperture Telescopes", The Astronomical Journal, vol. 140, no. 4, pp. 962–967, 2010. doi:10.1088/0004-6256/140/4/962.

[29] Martínez-Delgado, D., "Dwarfs Gobbling Dwarfs: A Stellar Tidal Stream around NGC 4449 and Hierarchical Galaxy Formation on Small Scales", The Astrophysical Journal, vol. 748, no. 2, 2012. doi:10.1088/2041-8205/748/2/L24.

[30] Martínez-Delgado, D., “A Stellar Tidal Stream Around the Whale Galaxy, NGC 4631”, The Astronomical Journal, vol. 150, no. 4, 2015. doi:10.1088/0004-6256/150/4/116.
[31]Johnston, K. V., Zhao, H., Spergel, D. N., and Hernquist, L., “Tidal Streams as Probes of the Galactic Potential”, The Astrophysical Journal, vol. 512, no. 2, pp. L109–L112, 1999. doi:10.1086/311876.
[32] Sanderson, R. E., Helmi, A., and Hogg, D. W., “Action-space Clustering of Tidal Streams to Infer the Galactic Potential”, The Astrophysical Journal, vol. 801, no. 2, 2015. doi:10.1088/0004-637X/801/2/98.
[33] Bovy, J., Bahmanyar, A., Fritz, T. K., and Kallivayalil, N., “The Shape of the Inner Milky Way Halo from Observations of the Pal 5 and GD--1 Stellar Streams”, The Astrophysical Journal, vol. 833, no. 1, 2016. doi:10.3847/1538-4357/833/1/31.
[34] Viel, M., Becker, G. D., Bolton, J. S., and Haehnelt, M. G., “Warm dark matter as a solution to the small scale crisis: New constraints from high redshift Lyman-α forest data”, Physical Review D, vol. 88, no. 4, 2013. doi:10.1103/PhysRevD.88.043502.
[35] Peter, A. H. G., Rocha, M., Bullock, J. S., and Kaplinghat, M., “Cosmological simulations with self-interacting dark matter - II. Halo shapes versus observations”, Monthly Notices of the Royal Astronomical Society, vol. 430, no. 1, pp. 105–120, 2013. doi:10.1093/mnras/sts535.
[36] Li, T. S., et al. “The Orbital and Chemical Properties of One Dozen Stellar Streams”, The Astrophysical Journal, vol. 928, no. 1, 2022. doi:10.3847/1538-4357/ac46d3.
[37] Panithanpaisal, N., Sanderson, R. E., Wetzel, A., Cunningham, E. C., Bailin, J., & Faucher- Giguere, C.-A. “The Galaxy Progenitors of Stellar Streams around Milky Way-mass Galaxies in the FIRE Cosmological Simulations”, The Astrophysical Journal, vol. 920(1), no. 10, 2021. doi: 10.3847/1538-4357/ac1109
[38] Crnojevic, D., Sand, D. J., Spekkens, K., Caldwell, N., Guhathakurta, P., McLeod, B., Seth, A., Simon, J. D., Strader, J., & Toloba, E.” The Extended Halo of Centaurus A: Uncovering Satellites, Streams, and Substructures”, The Astrophysical Journal, 823(1):19, 2016. doi: 10.3847/0004-637X/823/1/ 19.

[39] Dekel, A. and Silk, J., “The Origin of Dwarf Galaxies, Cold Dark Matter, and Biased Galaxy Formation”, The Astrophysical Journal, vol. 303, p. 39, 1986. doi:10.1086/164050.
[40] Yoon, J. H., Johnston, K. V., and Hogg, D. W., “Clumpy Streams from Clumpy Halos: Detecting Missing Satellites with Cold Stellar Structures”, The Astrophysical Journal, vol. 731, no. 1, 2011. doi:10.1088/0004-637X/731/1/58.
[41] Bonaca, A. and Hogg, D. W., “The Information Content in Cold Stellar Streams”, The Astrophysical Journal, vol. 867, no. 2, 2018. doi:10.3847/1538-4357/aae4da.
[42] Akhlaghi, M. and Ichikawa, T., “Noise-based Detection and Segmentation of Nebulous Objects”, The Astrophysical Journal Supplement Series, vol. 220, no. 1, 2015. doi:10.1088/0067-0049/220/1/1.
[43] Borlaff, A., “The missing light of the Hubble Ultra Deep Field”, Astronomy and Astrophysics, vol. 621, 2019. doi:10.1051/0004-6361/201834312.
[44] Trujillo, I., “Introducing the LBT Imaging of Galactic Halos and Tidal Structures (LIGHTS) survey. A preview of the low surface brightness Universe to be unveiled by LSST”, Astronomy and Astrophysics, vol. 654, 2021. doi:10.1051/0004-6361/202141603.
[45] Aihara, H., “Third data release of the Hyper Suprime-Cam Subaru Strategic Program”, Publications of the Astronomical Society of Japan, vol. 74, no. 2, pp. 247–272, 2022. doi:10.1093/pasj/psab122.
[46] Baldry, I. K., Glazebrook, K., and Driver, S. P., “On the galaxy stellar mass function, the mass-metallicity relation and the implied baryonic mass function”, Monthly Notices of the Royal Astronomical Society, vol. 388, no. 3, pp. 945–959, 2008. doi:10.1111/j.1365-2966.2008.13348.x.
[47] Grand, R. J. J., “The Auriga Project: the properties and formation mechanisms of disc galaxies across cosmic time”, Monthly Notices of the Royal Astronomical Society, vol. 467, no. 1, pp. 179–207, 2017. doi:10.1093/mnras/stx071.
[48] Vera-Casanova, A., “Linking the brightest stellar streams with the accretion history of Milky Way-like galaxies”, Monthly Notices of the Royal Astronomical Society, 2022. doi:10.1093/mnras/stac1636.
[49] Pearson, S., Starkenburg, T. K., Johnston, K. V., Williams, B. F.,

Ibata, R. A., and Khan, R., “Detecting Thin Stellar Streams in External Galaxies: Resolved Stars and Integrated Light”, The Astrophysical Journal, vol. 883, no. 1, 2019. doi:10.3847/1538-4357/ab3e06.
[50] de Boer, T. J. L., “A deeper look at the GD1 stream: density variations and wiggles”, Monthly Notices of the Royal Astronomical Society, vol. 477, no. 2, pp. 1893–1902, 2018. doi:10.1093/mnras/sty677.
[51] Besla, G., “Low Surface Brightness Imaging of the Magellanic System: Imprints of Tidal Interactions between the Clouds in the Stellar Periphery”, The Astrophysical Journal, vol. 825, no. 1, 2016. doi:10.3847/0004-637X/825/1/20.
[52] Hendel, D., Johnston, K. V., Patra, R. K., and Sen, B., “A machine-vision method for automatic classification of stellar halo substructure”, Monthly Notices of the Royal Astronomical Society, vol. 486, no. 3, pp. 3604–3616, 2019. doi:10.1093/mnras/stz1107
[53] Bonaca, A. and Hogg, D. W., “The Information Content in Cold Stellar Streams”, The Astrophysical Journal, vol. 867, no. 2, 2018. doi:10.3847/1538-4357/aae4da.
[54] Price-Whelan, A. M. and Bonaca, A., “Off the Beaten Path: Gaia Reveals GD-1 Stars outside of the Main Stream”, The Astrophysical Journal, vol. 863, no. 2, 2018. doi:10.3847/2041-8213/aad7b5.
[55] Helgason, K., Ricotti, M., and Kashlinsky, A., “Reconstructing the Near-infrared Background Fluctuations from Known Galaxy Populations Using Multiband Measurements of Luminosity Functions”, The Astrophysical Journal, vol. 752, no. 2, 2012. doi:10.1088/0004-637X/752/2/113.
[56] Kashlinsky, A., Arendt, R. G., Atrio-Barandela, F., Cappelluti, N., Ferrara, A., and Hasinger, G., “Looking at cosmic near-infrared background radiation anisotropies”, Reviews of Modern Physics, vol. 90, no. 2, 2018. doi:10.1103/RevModPhys.90.025006.
[57] Zemcov, M., “High Spectral Resolution Measurement of the Sunyaev-Zel'dovich Effect Null with Z-Spec”, The Astrophysical Journal, vol. 749, no. 2, 2012. doi:10.1088/0004-637X/749/2/114.
[58] Cooray, A., “Near-infrared background anisotropies from diffuse intrahalo light of galaxies”, Nature, vol. 490, no. 7421, pp. 514–516, 2012. doi:10.1038/nature11474.
[59] Purcell, C. W., Bullock, J. S., and Zentner, A. R., “The

metallicity of diffuse intrahalo light", Monthly Notices of the Royal Astronomical Society, vol. 391, no. 2, pp. 550–558, 2008. doi:10.1111/j.1365-2966.2008.13938.x.

[60] Simon, J. D., "The Faintest Dwarf Galaxies", Annual Review of Astronomy and Astrophysics, vol. 57, pp. 375–415, 2019. doi:10.1146/annurev-astro-091918-104453.

[61] Pearson, S., "The Hough Stream Spotter: A New Method for Detecting Linear Structure in Resolved Stars and Application to the Stellar Halo of M31", The Astrophysical Journal, vol. 926, no. 2, 2022. doi:10.3847/1538-4357/ac4496.

[62] Dekel, A. and Birnboim, Y., "Galaxy bimodality due to cold flows and shock heating", Monthly Notices of the Royal Astronomical Society, vol. 368, no. 1, pp. 2–20, 2006. doi:10.1111/j.1365-2966.2006.10145.x.

[63] Kutner, M. L., "Results of the ESO-SEST key programme: CO in the Magellanic Clouds. VI. The 30 DOR Complex", Astronomy and Astrophysics Supplement Series, vol. 122, pp. 255–266, 1997. doi:10.1051/aas:1997334.

[64] Johansson, L. E. B., "Results of the SEST key programme: CO in the Magellanic Clouds. VII. 30 Doradus and its southern H II regions", Astronomy and Astrophysics, vol. 331, pp. 857–872, 1998.

[65] Santos-Santos, I. M. E., Navarro, J. F., and McConnachie, A., "The Tucana dwarf spheroidal: a distant backsplash galaxy of M31?", arXiv e-prints, 2022.